8-6-2015 12:00 AM

Characterization of Maga Expression and Iron Uptake in P19 Cells: Implications for Use as a Gene-Based Contrast Agent

Linshan Liu
The University of Western Ontario

Supervisor
Donna Goldhawk
The University of Western Ontario Joint Supervisor
Lisa Hoffman
The University of Western Ontario

Graduate Program in Medical Biophysics
A thesis submitted in partial fulfillment of the requirements for the degree in Master of Science
© Linshan Liu 2015

CHARACTERIZATION OF MAGA EXRESSION AND IRON UPTAKE IN P19 CELLS:

IMPLICATIONS FOR USE AS A GENE-BASED CONTRAST AGENT FOR MRI

(Thesis format: Monograph)

by

Linshan Liu

Graduate Program in Medical Biophysics

Collaborative Graduate Program in Molecular Imaging

A thesis submitted in partial fulfillment
of the requirements for the degree of
Master of Science

The School of Graduate and Postdoctoral Studies
The University of Western Ontario, London, Ontario, Canada
© Linshan Liu, 2015

Abstract

Magnetic resonance imaging (MRI) is one of the non-invasive imaging modalities used in longitudinal cell tracking. Previous studies suggest that MagA, a putative iron transport protein from magnetotactic bacteria, is a useful gene-based magnetic resonance contrast agent. Hemagglutinin (HA)-tagged MagA was stably expressed in undifferentiated embryonic mouse teratocarcinoma, multipotent P19 stem cells to provide a suitable model for tracking these cells during differentiation. Western blot and immunocytochemistry confirmed the expression and membrane localization of MagA-HA in P19 cells. Elemental iron analysis using inductively-coupled plasma mass spectrometry revealed significant iron uptake in both parental and MagA-HA-expressing P19 cells, cultured in the presence of iron-supplemented medium. Withdrawal of this extracellular iron supplement revealed unexpected iron export activity in P19 cells, which MagA-HA expression attenuated. The influence of iron supplementation on parental and MagA-HA-expressing cells was not reflected by longitudinal relaxation rates. Measurement of transverse relaxation rates (R2* and R2) reflected changes in total cellular iron content. In particular, the reversible component R2′ (R2* − R2) provided a moderately strong correlation to amount of cellular iron, normalized to amount of protein.

Keywords

Acknowledgments

In completing my M.Sc. and throughout my educational career, there are numerous people that deserve my grateful thanks. As such, I would like to briefly acknowledge them for helping me to achieve this milestone.

I would first like to thank my supervisors Dr. Donna Goldhawk and Dr. Lisa Hoffman. I have spent a considerable amount of time in your labs, as a graduate student working towards my M.Sc. Dr. Goldhawk, thank you for always trying to help while things went south. Thanks very much for all your patience and your time to help me. Dr. Hoffman, thank you very much for listening to all my questions and doing your best to try to help me make my research move forward. Thank you all for the trust to let me work in your lab to explore new areas of research. Lastly, thanks for your continued support and guidance along the way. Your continued passion and excitement for research is inspiring and has motivated me a great deal in graduate school.

Next, I would like to thank my committee advisors Dr. Frank Prato, Dr. Terry Thompson and Dr. Savita Dhanvantari for all the advice and guidance with my research and help in my study. Dr. Thompson and Dr. Dhanvantari, thank you for not only providing valuable advice, but also for taking your time to read my thesis. In addition, thank you all for being on my qualifying exam committee.

I would also like to thank the many members of the Goldhawk and Hoffman Lab (past and present) who have helped to create a great environment to conduct research. Thanks for your advice on my research, and for advising me about various experiments. I particularly would like to thank Becky McGirr who was always being so willing to help and share advice based on her experiences in the lab. I truly appreciate it. Thanks also to Karina Quiaoit, Kelly Gutpell, Anindita Sengupta, Casey Lee, Andrew Bondoc, Sarah Donnelly and many others in the lab who have made research life enjoyable.

I'm especially grateful to my uncle, Junmin Liu. Thank you so much for all your support. Thank you for picking me up at the airport when I first moved to Canada. Without

your kindly support, I couldn't settle in Canada and be ready to put all my energy into my study in such a short period of time. In addition, thank you so much for always trying to help in any way you can. Your motivation, intelligence, and dedication really inspire me. Lastly, thank you so much for your patience and for continually challenging me throughout my education.

My final thanks are reserved for my parents for their unconditional love and support throughout my life. Thank you for always being on my side to cheer me up. I'm so grateful for the chance to study in Canada, which wouldn't happen without your support. Mom, your passion, integrity and work ethic have always had a great impact on me. Thank you so much for all the advice, encouragement, selflessness, and kindness. Dad, thank you so much for always comforting, challenging, and sharing your own life experience. Thanks so much for believing in me and always being there to listen, support and encourage me. To both of my parents, I could not have achieved this without you!

Table of Contents

List of Tables

List of Figures

List of Abbreviations

αMEM	Alpha-minimum essential medium
AVG	Average
β –gal	β -galactosidase
B_0	External magnetic field
BLI	Bioluminescence imaging
BSA	Bovine serum albumin
CT	X-ray computed tomography
ER	Endoplasmic reticulum
FID	Free induction decay
FBS	Fetal bovine serum
Fpn1	Ferroportin 1
Fe(II)	Ferrous iron
GFP	Green fluorescent protein
HA	Hemagglutinin
ICC	Immunocytochemistry
ICP-MS	Inductively-coupled plasma mass spectrometry
Ig	Immunoglobulin
Kb	kilobase

NMR	Nuclear magnetic resonance
MAI	Magnetosome island
MS-1	M. magnetotacticum strain
M_0	Net magnetization
MR	Magnetic resonance
MRI	Magnetic resonance imaging
MRS	Magnetic resonance spectroscopy
M.W.	Molecular weight
M	Net magnetization
M_z	Longitudinal magnetization
M_{xy}	Transverse magnetization
PBS	Phosphate-buffered saline
PET	Positron emission tomography
R2	Irreversible component of transverse relaxation rate
R2*	Transverse relaxation rate
R2′	Reversible component of transverse relaxation rate
ROI	Region of interest
SD	Standard deviation
SEM	Standard error of the mean

SPECT	Single photon emission computed tomography
SPIO	Superparamagnetic iron oxide
T	Tesla
T1	Longitudinal relaxation time
T2	Irreversible component of total effective transverse decay
T2*	Total effective transverse decay
T2′	Reversible component of total effective transverse decay
TBS	Tris-buffered saline
TBS-T	Tris-buffered saline/0.1% tween 20
TE	Echo time
TR	Repetition time
TI	Inversion time
WGA	Wheat germ agglutinin

Chapter 1

1.1 Molecular and Cellular Imaging

Broadly-speaking, molecular imaging is the *in vivo* evaluation of biological processes at the cellular and molecular level [1]. By using molecular imaging techniques, our ability to monitor cells and specific proteins within a living organism has been tremendously improved [2]. For example, molecular imaging can be used to locate specific groups of cells or the level of a given protein of interest in the cell, permitting noninvasive characterization of the progression of disease(s) and development of biomarkers of these processes [3]. In addition, the efficiency of treatment in small-animal models of human disease can be assessed using molecular imaging [4]. Stem cell therapy, for example, is a promising treatment for multiple diseases, such as neurodegenerative disease and heart disease; however, in order to understand the fundamental behaviour of stem cells, different molecular imaging modalities have been developed to better understand stem cell survival, distribution and function in the targeted regions [5]. Many traditional imaging modalities such as ultrasound, x-ray computed tomography (CT) and magnetic resonance imaging (MRI) are based on nonspecific macroscopic changes that distinguish pathological tissues from healthy ones but do not identify changes in gene expression and other molecular interactions responsible for the disease [1]. To address this shortcoming, molecular imaging attempts to exploit specific probes with intrinsic contrast agent properties [2]. This transition from nonspecific to specific labeling represents an outstanding improvement in targeting the disease process, providing new opportunities for understanding integrative biology and for detecting and characterizing disease at earlier stages.

Molecular imaging has been applied to long-term studies using different imaging modalities such as optical imaging, CT, positron emission tomography (PET), single photon emission computed tomography (SPECT), ultrasound and MRI. Each of the imaging modalities has inherent advantages and limitations. Optical imaging is useful for detecting the expression of fluorescent proteins, such as green fluorescent protein (GFP),

or the bioluminescent activity of luciferase (*e.g.* firefly luciferase), which is useful for understanding aspects of intracellular activity. GFP, as an example, was identified in 1962; explored as a reporter gene in 1992 [6]; and then later examined for its ability to maintain fluorescence in a variety of organisms [6, 7]. However, the use of GFP for monitoring molecular changes *in vivo* is limited by the depth of light penetration and low resolution (2-3 mm for optical fluorescence imaging and 3-5 mm for optical bioluminescence) [2]. By comparison, PET and MRI have also been used to monitor gene expression in living organisms, with the advantage of satisfactory depth of interrogation.

Nuclear medicine techniques use small amounts of radioactive material (radiopharmaceuticals) to diagnose and treat diseases. PET has been used to evaluate the metabolism of a particular organ or tissue by attaching different radioactive atoms, such as ^{18}F, ^{15}O or ^{11}C, to substances that are naturally consumed by the target organ or tissue. Commonly used substances include ^{18}F-fluorodeoxyglucose [1] and ^{11}C-methionine [8]. By using the radiotracers, physiological and biochemical information can be obtained. Although spatial resolution is relatively poor with nuclear medicine platforms (namely PET and SPECT), co-registration with CT or MRI provides a hybrid imaging solution (PET/CT, SPECT/CT, PET/MRI). The short half-life of medical radiotracers is essential for the clinical utility of ionizing radiation but constrains direct radiolabelling of cells for long periods of time (*e.g.* Indium-111 has a half-life of 2.8 days) and the number of repeat imaging sessions.

MRI has a number of advantages over other imaging modalities: no ionizing radiation is needed; tissue is imaged at high spatial resolution (25-100 µm in preclinical settings, and approximately 1 mm in clinical settings); and depth of penetration is not a concern [9]. Over the past two decades, MRI has been used in longitudinal studies [10, 11] for (repetitive) monitoring of stem cell engraftment, tumor growth and metastasis, changes in pancreatic beta cell function during diabetes and cardiac cell activity after heart attack [12]. Yet, despite all of its strengths, MRI fails to track cellular and molecular activities with the sensitivity that has been achieved in optical imaging using reporter genes such as the green fluorescent protein and luciferase [1] or in PET using radiotracers. Here, the definition of sensitivity is the minimum concentration of imaging

agent that can be detected. The sensitivity of MRI is approximately 10^{-3}-10^{-5} molar, which is much lower than the sensitivity of PET (10^{-11}-10^{-12} molar), optical fluorescence imaging (10^{-9}-10^{-12} molar) and optical bioluminescence imaging (10^{-15}-10^{-17} molar). In order to develop molecular MRI, cells must be labeled with a contrast agent to improve cell tracking and the detection of molecular activity [13]. To understand how contrast agents can improve MRI, information about how MRI works and why contrast agents influence the MR signal will be explained below.

1.1.1   MRI Relaxometry

Relaxometry is the study or measurement of nuclear magnetic resonance (NMR) relaxation parameters. NMR is a phenomenon that can be observed when a group of nuclei containing an odd number of protons and/or neutrons is placed within a strong magnetic field. When combined with spatial encoding methods, NMR leads to MRI: a tool that can provide images of the macroscopic structure of biological systems. Historically the word 'nuclear' was dropped from the nomenclature of this imaging modality to avoid any misconceptions that there was ionizing radiation involved as in Nuclear Medicine. Since more than 60 % of the human body is water (H_2O), hydrogen is the most abundant element imaged in MRI. A hydrogen atom is composed of a nucleus (with 1 proton and no neutrons) and a single orbital electron. The hydrogen ion (H^+) is often referred to as a 'proton' since that is the only particle left if the electron is removed. Classically, protons are considered spinning charged particles with a small magnetic moment typically denoted by the symbol µ. Without an external magnetic field, the nuclear moments are in random directions and thus, the vector sum of the nuclear magnetic moments (net magnetization, M) will be zero.

When nuclei with magnetic moments are placed in a strong external magnetic field (B0), most magnetic moments will still have a random orientation [14] but there will be a small net magnetic moment created (vector sum of all the magnetic moments) aligned parallel (low energy state) to B0. Thus, M becomes non-zero and is along the direction of the applied magnetic field [15].

In addition, when protons are placed within B_0, they experience a torque caused by the interaction between the spins and the magnetic field, and start to precess at an angular frequency defined as the Larmor frequency (ω_0) and determined by the Larmor equation:

$$\omega_0 = \gamma \times B_0 \hspace{3cm} [1.1]$$

In Equation 1.1, γ is the gyromagnetic ratio, which is equal to 42.576 MhzT^{-1} for hydrogen. Thus, the precession frequency is linearly related to the strength of the magnetic field. For example, clinical MRI scanners are usually 1.5 Tesla (T) or 3 T and provide a precession frequency for hydrogen of approximately 64 MHz and 128 MHz, respectively.

In order to detect the MRI signal, an external oscillating magnetic field (B_1) is applied perpendicular to B_0, *i.e.* in the x-y plane. The oscillation frequency of B_1 is equal to ω_0. M will rotate (or precess) about B1 with a frequency (ω_1) equal to γB1. Since B1 is oscillating at the Larmor frequency, effectively it is rotating at the same frequency as the 'spins'. The net magnetization rotates away from the Z-axis towards the X-Y plane. The angle of rotation (α) of M is dependent on the duration and amplitude of B_1. A 90-degree pulse occurs when B_1 is on long enough to cause a $\pi/2$ rotation of M. This transient B_1 magnetic field is known as a radio frequency (RF) pulse since ω_1 is in the MHz range. Once the RF pulse is turned off, the magnetic moments will continue to precess at the Larmor frequency and M will return exponentially to its original value parallel with B_0, which is defined as the equilibrium state. The process of returning to the equilibrium state is referred to as 'longitudinal' relaxation. During relaxation, the nuclei lose energy by exchange of energy with lattice around the nuclei. The time it takes M to return to 63% of its original value following a 90-degree pulse is called T1. In NMR, this is often referred to as the spin-lattice relaxation time as the spins give up the 'extra' energy they receive to the surroundings or 'lattice'. The lattice produces transient magnetic fields (usually due to molecular motion) at the Larmor frequency [15].

Following the termination of the B_1 RF pulse, the magnetization in the X-Y plane (Mxy) will exponentially decay to 0 (excluding the T1 relaxation) and the characteristic

time (for Mxy to irreversibly decay to 37% of its original magnitude) for this decay is called the transverse relaxation time (T2). This assumes that the only mechanism is random fluctuations in the local magnetic field. In reality what is normally observed in the free induction decay (FID) is the total effective transverse decay (T2*), which is a combination of microscopic de-phasing (T2) and local magnetic field inhomogeneities (T2′). T1, T2 and T2* are converted to decay rates (R1 = 1/T1, R2 =1/T2 and R2* = 1/T2*). The reversible component, R2′, is the difference between R2* and the irreversible component, R2 (R2′ = R2* − R2). Related equations are thoroughly described in section 2.2.5.4.

1.1.2 Contrast Agents for Cell Tracking with MRI Relaxometry

Contrast agents can significantly improve the quality of a biomedical image and enable targeted or functional imaging. MRI contrast agents are roughly categorized into two groups: exogenous, such as gadolinium (Gd) [16], magnesium (Mg) [17] and super-paramagnetic iron oxide (SPIO) particles [18] and endogenous agents, such as tyrosinase [19], β-galactosidase (β-gal), ferritin and MagA. Most exogenous MRI contrast agents do not directly contribute to the signal but alter the signal of the surrounding water protons through their effects on relaxation rates.

Exogenous contrast agents can be roughly divided into two types: those that have an influence on R1, such as gadolinium or manganese[20], and those that have an influence on R2, such as superparamagnetic iron oxide (SPIO) particles [18]. Iron introduces local magnetic field inhomogeneity (*i.e.*, changes in R2′) and iron oxide-based contrast has been increasingly used in MRI either as direct contrast agents *in vivo*, or as indicators for monitoring specific proteins *in vitro* and *in vivo*. SPIO nanoparticles are commonly used in the research setting and in clinical trials [13], often to label cells for tracking with MRI [21]. Cells are usually labeled with SPIO *ex vivo* and imaged following administration. Since the iron oxide nanoparticles are diluted by cell division, SPIO-induced contrast may be lost over time.

Compared to exogenous contrast agents, endogenous contrast agents can be tracked over a long term without dilution caused by cell proliferation. Expression of MRI reporter genes, which are under the control of a regulatory promoter, can be either easily detectable or capable of storing certain elements that can improve the MRI contrast. Genetically engineered cells expressing MRI reporter genes provide information on the location, fluctuation and duration of transcriptional activity in living cells and animals. Iron-related endogenous contrast agents are produced by the cell's genetic machinery in order to modulate the uptake, storage, and processing of iron [12]. Iron can act as a paramagnetic metal depending on its oxidation and structure. In addition, iron concentration will have an impact on MRI contrast. A few mammalian iron handling proteins have been studies as potential MRI reporters [22]. For example, transferrin receptor (TfR) and ferritin, present in mammalian cells, were investigated by researchers for the capability of developing T2/T2* contrast on MR images [12, 23-25]. Genes from magnetotactic bacteria will be discussed in Section 1.2.

1.2   Role of MagA Expression in MRI

1.2.1   Magnetotactic Bacteria

Magnetotactic bacteria are a group of prokaryotes that can synthesize magnetic crystals called "magnetosomes" and typically arrange these in a chain within the cell. These bacteria move along an external magnetic field through a process called magnetotaxis. Blakemore *et al*. initially identified this unique phenomenon in the microorganisms collected from the salt marshes of Cape Cod in 1975 and called them magnetotactic bacteria after discovering the magnetosome structure within the bacteria [26].

Magnetosome crystals are either composed of the magnetite (Fe_3O_4), or greigite (Fe_3S_4), depending on the species. In comparison to mammalian ferritin, which is a ferrihydrite core surrounded by protein, the relaxivity of magnetite or maghemite particles in solution is approximately 700 times more than that of ferritin in solution or tissue. There are approximately 28 genes involved [27] in the formation of

magnetosomes. Although a full understanding of the process of magnetosome formation is lacking, many applications of the unique magnetosome compartment have been postulated [28], including its utility in cell tracking with MRI [12, 23, 24, 29].

1.2.2   MagA in Magnetotactic Bacteria

MagA was one of the genes originally thought to be involved in magnetosome formation. Nakamura *et al*. reported that production of *MagA* may be involved in the iron biomineralization process [30]. When MagA was expressed in *E. coli*, inverted membrane vesicles within cells were shown to transport ferrous iron (Fe(II)) in an energy-dependent manner, resulting in Fe(II) accumulation in the vesicle. These observations suggested that MagA may function as an H+/Fe(II) antiporter in *M. magneticum* sp. AMB-1 [31]. A full genomic analysis of AMB-1 confirmed that deletions in *MagA* were present among a set of nonmagnetic mutants. Thus, MagA may play a role in magnetosome formation, although further study is required to delineate its exact function. More recently, a study from Uebe *et al*. showed that *MagA* is not an essential magnetosome gene [32]. Nevertheless, MagA is a putative iron transport protein and a candidate for MRI reporter gene expression [12, 23, 24, 29, 33].

1.2.3   Using MagA for MRI-based Cell Tracking

MagA and its potential utility in MR cell tracking have been reported and initial results indicate that this technique is promising. The first report on MagA-expressing cell tracking used human embryonic kidney (HEK) 293 FT cells to express MagA under the control of an inducible promoter [29]. Zurkiya *et al*. introduced *MagA* from species MS-1 into a doxycycline-responsive gene construct, and generated a stably expressing cell line in 293FT cells. MRI showed that *MagA*-derived contrast can be formed *in vivo* in response to iron supplementation and can be used to track cells expressing M*agA*. They compared the iron uptake in MagA-expressing cells in three different doxycycline induction conditions (0, 0.5, 2 µg/ml) and found that with same amount of iron supplementation (200 µM for four days), different amounts of doxycycline changed the

iron content of the cells. They also presented electron microscopic and X-ray powder diffraction data as evidence of the ability of MagA-expressing 293FT cells to produce magnetite nanoparticles. Goldhawk *et al*. expressed *MagA* from species AMB-1 in the mouse neuroblastoma N2A cell line and used 11 T micro MRI and a novel dual echo sequence (spin echo at an echo time (TE) of 5 ms and gradient echo at TE 15 ms) to acquire three-dimensional MRI [33]. An important step in demonstrating the utility of MagA-derived MR contrast for cell tracking is to show that MagA expression will lead to changes in the relaxation rates, especially the transverse relaxation rates (R2*, R2 and R2′). Expression of MagA in N2A cells generates intracellular contrast for MRI detection at 11 T as measured by the decay rates [33].

Sengupta *et al*. compared the expression of MagA in MDA-MB-435 cells with the overexpression of modified ferritin subunits, in which both heavy chain (HF) and light chain (LF) lack iron response elements [23]. Their results showed that only transverse relaxation rates were significantly higher in iron-supplemented, MagA- and HF+LF-expressing cells compared to non-supplemented cells and the parental control. R2* provided the greatest absolute difference and R2′ showed the greatest relative difference, consistent with the notion that R2′ may be a more specific indicator of iron-based contrast than R2, as observed in brain tissue. Upon iron supplementation, the ratio of iron and zinc increased about 20-fold in both MagA- and HF+LF-expressing cells, while the amount of transferrin receptor expressed in these cells decreased more than 6-fold [23]. Thus, despite a decrease in iron import, MagA activity resulted in an increase in cellular iron content, comparable to unregulated ferritin storage. These results highlight the potential of magnetotactic bacterial gene expression for improving MR contrast.

Understanding the MRI relaxation mechanism in these expression systems is important for developing magnetosome-associated genes as cell tracking tools. To optimize cell detection and specificity, develop quantification methods, and refine gene-based iron contrast, a study by Lee *et al.* investigated the properties of mammalian cells over-expressing MagA using 9.4 T NMR [34]. In this study, the relationship between R2 and interecho time was examined in both parental MDA-MB-435 and MagA-expressing cells cultured in the presence and absence of iron supplementation. The relationship

between R2 and interecho time was analyzed using the Carr-Purcell-Meiboom-Gill spin echo sequence [35] and a model based on water diffusion in weak magnetic field inhomogeneities [36] as well as a fast-exchange model [37]. Iron levels were assessed with inductively coupled plasma mass spectrometry (ICP-MS). As expected from a previous work [23], iron levels in iron-supplemented, MagA-expressing cells were higher than in the other cell conditions. With regard to NMR, increases in R2 with increasing interecho time were larger in iron-supplemented cells compared to unsupplemented cells and the parental control. These findings provide insight into the high field relaxation mechanisms in these MagA-expressing cells, which should be valuable for optimizing MRI contrast for long-term cell tracking and monitoring of cellular activities.

1.3 Overview of This Thesis

1.3.1 Hypothesis

In this thesis, we hypothesized that MagA-induced iron accumulation can generate detectable *in vivo* contrast, measurable by MRI relaxometry, in the P19 model of stem cell behaviour.

1.3.2 Motivation

This thesis is motivated by the potential of stem cell therapy. Numerous animal studies have shown success in delivering stem cells to treat a variety of diseases. Clinical studies in stem cell therapy are promising. For example, recent studies show some success in cell transplantation in the infarcted heart [38, 39].

MRI is widely used in cell tracking. Specifically, cells labeled with magnetically visible contrast agents, which are either exogenous or endogenous, have great potential to fulfill this goal. Using exogenous contrast agents, however, there is a limitation in localizing those labeled cells over the long term once delivered to the organ. In order to study or develop effective cell therapy, researchers have focused on genetically

modifying cells to take up iron. Compared to other techniques like labelling the cells with exogenous contrast agents (SPIOs), MagA overexpression can provide stable labelling for long-term *in vitro* and *in vivo* study.

1.3.3 Choice of Cell Line

The cell line used in all the experiments of this thesis is a mouse embryonic teratocarcinoma denoted P19. These cells possess multipotent stem cell characteristics and can differentiate into the three germ layers: endoderm, mesoderm, and ectoderm, as specified by different chemical treatments [40, 41].

P19 cells grow rapidly without feeder cells and are effectively transfected with DNA encoding recombinant genes. Addition of appropriate antibiotics to the cell culture readily permits isolation of P19 cells stably expressing a gene of interest.

1.3.4 Thesis Objectives

The path for testing the hypothesis includes multiple sequential objectives. The first objective (1) is to ensure that the *MagA* gene from magnetotactic bacteria can be inserted into P19 cells and that *MagA*-transfected P19 cells are able to stably express MagA. This was achieved with a hemagglutinin (HA)-tagged *MagA* expression construct. To detect MagA protein, we performed Western blot analysis using a commercial HA antibody as well as immunocytochemical localization.

The second objective (2) aims to demonstrate the level of iron uptake in undifferentiated P19 cells and in the presence and absence of MagA-HA expression. Iron supplementation was provided to both types of cells. To measure the total iron content in parental and MagA-HA-expressing cells, ICP-MS analysis was used. We expected that MagA-HA-expressing P19 cells would incorporate more iron than parental cells as reported for other cell types [12, 23, 29, 33].

The third objective (3) is to determine whether undifferentiated, iron-supplemented parental and MagA-HA-expressing P19 cells can be distinguished using MRI relaxometry. For both parental and MagA-HA-expressing P19 cells, transverse

relaxation rates (R2*, R2 and R2′) were measured and compared to total cellular iron content.

1.4 References

1. Massoud, T. and S. Gambhir, *Molecular imaging in living subjects: seeing fundamental biological processes in a new light.* Genes Dev, 2003. **17**: p. 545-580.

2. James, M.G., SS, *A moleculae imaging primer: modalities, imaging agents, and applications.* Physiol Rev, 2012. **92**(2): p. 897-965.

3. Madu, C.L., Y, *Novel diagnostic biomarkers for prostate cancer.* J Cancer, 2010. **1**: p. 150-77.

4. Du, Y.Z., Q; Jing, L; Liang, X; Chi, C; Li, Y; Yang, X; Dai, Z; Tian, J, *GX1-conjugated poly(lactic acid) nanoparticles encapsulating Endostar for improved in vivo anticolorectal cancer treatment.* Int J Nanomedicine., 2015. **10**: p. 3791-802.

5. Godier-Furnémont, A.T., Y; Kollaros, M; Eng, G; Morales, A; Vunjak-Novakovic, G; Johnson, LL, *Noninvasive imaging of myocyte apoptosis following application of a stem cell-engineered delivery platform to acutely infarcted myocardium.* J Nucl Med, 2013. **54**(6): p. 977-83.

6. Prasher, D.E., VK; Ward, WW; Prendergast, FG; Cormier, MJ, *Primary structure of the Aequorea victoria green-fluorescent protein.* Gene, 1992. **111**(2): p. 229-33.

7. Inouye, S.T., FI, *Aequorea green fluorescent protein. Expression of the gene and fluorescence characteristics of the recombinant protein.* FEBS Lett, 1994. **341**(2-3): p. 277-80.

8. Rheims, S.R., S; Bouvard, S; Bernard, E; Streichenberger, N; Guenot, M; LeBars, D; Hammers, A; Ryvlin, P, *Accuracy of distinguishing between dysembryoplastic neuroepithelial tumors and other epileptogenic brain neoplasms with [^{11}C]methionine PET.* Neuro Oncol, 2014. **16**(10): p. 1417-26.

9. Alam, S.S., AS; Richards, J; Lang, NN; Barnes, G; Joshi, N; MacGillivray, T; McKillop, G; Mirsadraee, S; Payne, J; Fox, KA; Henriksen, P; Newby, DE; Semple, SI, *Ultrasmall superparamagnetic particles of iron oxide in patients with acute myocardial infarction: early clinical experience.* Circ Cardiovasc Imaging, 2012. **5**(5): p. 559-65.

10.   Jeff WM, B.I.D., Duncan; Joseph A, Frank, *In vivo magnetic resonance tracking of magnetically labeled cells after transplantation.* J Cereb Blood Flow Metab, 2002. **22**(8): p. 899-907.

11.   Bulte, J., *In vivo MRI cell tracking: clinical studies. .* AJR Am J Roentgenol., 2009. **193**(2): p. 314-25.

12.   Goldhawk, D.R., R; Sengupta, A; Gelman, N; Prato, FS, *Using the magnetosome to model effective gene-based contrast for magnetic resonance imaging.* Wiley Interdiscip Rev Nanomed Nanobiotechnol, 2012. **4**(4): p. 378-88.

13.   Li, L.W., Jiang; Kui, Luo; Hongmei, Song; Fang, Lan; Yao, Wu; Zhongwei, Gu, *Superparamagnetic iron oxide nanoparticles as MRI contrast agents for non-invasive stem cell labeling and tracking.* Theranostics, 2013. **3**(8): p. 595-615.

14.   Hanson, L., *Is quantum mechanics necessary for understanding magnetic resonance?* Concepts in Magnetic Resonance. Part A, 2008. **32A**(5): p. 329-40.

15.   Haacke, E.M.B., Robert F; Thompson, Michael; Venkatesan, Ramesh *Magnetic resonance imaging: Physical principles and sequence design.* New York: J. Wiley & Sons, 1999: p. 1-15.

16.   Zhou, Z.L., ZR, *Gadolinium-Based Contrast Agents for MR Cancer Imaging.* Wiley Interdiscip Rev Nanomed Nanobiotechnol, 2013. **5**(1): p. 1-18.

17.   Aoki, I.W., YJ; Silva, AC; Lynch, RM; Koretsky, AP, *In vivo detection of neuroarchitecture in the rodent brain using manganese-enhanced MRI.* Neuroimage., 2004. **22**(3): p. 1046-59.

18.   Thorek, D.C., AK; Czupryna, J; Tsourkas, A, *Superparamagnetic iron oxide nanoparticle probes for molecular imaging.* Ann Biomed Eng., 2006. **34**(1): p. 23-38.

19.   H, A.H., Stöppler; F, Nocken; JT, Heverhagen; B, Kleb; F, Czubayko; KJ, Klose, *In vitro MR imaging of regulated gene expression.* Radiology, 2003. **228**(2): p. 488-92.

20.   Kirsch, J., *Basic principles of magnetic resonance contrast agents.* Top Magn Reson Imaging, 1991. **3**(2): p. 149-56.

21.   Carlos, F., Geraldesan; Sophie, Laurent, *Classification and basic properties of contrast agents for magnetic resonance imaging. .* Contrast Media MoI. Imaging, 2009. **4**: p. 1-23.

22.   Gilad, A.Z., K; McMahon, MT; van Zijl, PC; Neeman, M; Bulte, JW, *MRI reporter genes.* J Nucl Med, 2008. **49**(12): p. 1905-8.

23.   Sengupta, A.Q., K; Thompson, RT; Prato, FS; Gelman, N; Goldhawk, DE, *Biophysical features of MagA expression in mammalian cells: implications for MRI contrast.* Front Microbiol., 2014. **5**(29).

24.   Cho, I.M., SP; Paudyal, R; Piotrowska-Nitsche, K; Cheng, PH; Zhang, X; Mao, H; Chan, AW, *Longitudinal monitoring of stem cell grafts in vivo using magnetic resonance imaging with inducible MagA as a genetic reporter.* Theranostics, 2014. **4**(10): p. 972-89.

25.   Zhang, X.R., BN; Harris, SS; Hu, XP, *A Bacterial Gene, mms6, as a New Reporter Gene for Magnetic Resonance Imaging of Mammalian Cells.* Mol Imaging., 2014. **13**(0): p. 1-12.

26.   Blakemore, R., *Magnetotactic bacteria.* Science, 1982. **190**(4212): p. 377-379.

27.   Nudelman, H. and R. Zarivach, *Structure prediction of magnetosome-associated proteins.* Front Microbiol, 2014. **5**: p. article 9.

28.   Araujo, A.A., F; Silva, KT; Bazylinski, DA; Lins, U, *Magnetotactic bacteria as potential sources of bioproducts.* Mar Drugs, 2015. **13**(1): p. 389-430.

29.   Zurkiya, O.C., AW; Hu, X, *MagA is sufficient for producing magnetic nanoparticles in mammalian cells, making it an MRI reporter.* Magn Reson Med., 2008. **59**(6): p. 1225-31.

30.   Nakamura, C.B., JG; Sode, K; Matsunaga, T, *An iron-regulated gene, MagA, encoding an iron transport protein of Magnetospirillum sp. strain AMB-1.* J Biol Chem, 1995. **270**(47): p. 28392-6.

31.   Faivre, D.S., D, *Magnetotactic bacteria and magnetosomes.* Chem Rev, 2008. **108**(11): p. 4875-98.

32.   Uebe, R., V. Henn, and D. Schuler, *The MagA protein of Magnetospirilla is not involved in bacterial magnetite biomineralization.* J Bacteriol, 2012. **194**: p. 1018-23.

33.   Goldhawk, D.L., C; McCreary, CR; McGirr, R; Dhanvantari, S; Thompson, RT; Figueredo, R; Koropatnick, J; Foster, P; Prato, FS, *Magnetic resonance imaging of cells overexpressing MagA, an endogenous contrast agent for live cell imaging.* Mol Imaging, 2009. **8**(3): p. 129-39.

34.   Lee, C., *Quantitative analysis of relaxation rate dependence on interecho time in MagA-expressing, iron-labeled cells.* Master Thesis, Western University, 2014.

35.   Schurr, J.F., BS; Diaz, R; Robinson, BH, *Manifestations of slow site exchange processes in solution NMR: a continuous Gaussian exchange model.* J Magn Reson, 1999. **140**(2): p. 404-31.

36.   Jensen, J.C., R, *MR imaging of microvasculature. .* Magn Reson Med., 2000. **44**(2): p. 224-30.

37.   Z, L.S., Meiboom, *Nuclear magnetic resonance study of the protolysis of trimethylammonium ion in aqueous solution—order of the reaction with respect to solvent.* J. Chem. Phys., 1963. **39**: p. 366-370.

38.   Durrani, S.K., M; Ashraf, M; Haider, KH, *Skeletal myoblasts for cardiac repair.* Regen Med, 2010. **6**(5): p. 919-32.

39.   Shiba, Y.H., KD; Laflamme, MA, *Cardiac applications for human pluripotent stem cells.* Curr Pharm Des, 2009. **15**(24): p. 2791-806.

40.   McBurney, M., *Clonal lines of teratocarcinoma cells in vitro: differentiation and cytogenetic characteristics.* J Cell Physiol., 1976. **89**(3): p. 441-55.

41.   Gail R, M.M.J., Evans, *Multiple differentiation of clonal teratocarcinoma stem cells following embryoid body formation in vitro.* Cell, 1975. **6**(4): p. 467-474.

Chapter 2

2.1. Introduction

Molecular Imaging has been used in the characterization and measurement of biological processes [1] by exploiting molecular probes as contrast agents for imaging modalities like CT, MRI and PET [2]. For longitudinal cell tracking by MRI, a few techniques for tracking magnetically labeled cells have been proposed, including gene-based approaches [3]. Previous studies suggest that MagA, a putative iron-transport protein found in magnetotactic bacteria, can be used as an endogenous contrast agent for MRI [4]. These reports indicate that MagA is involved in increasing cellular iron content, as confirmed by MR relaxation rates and elemental analysis [5-7].

In the present study, we provide the first report of MagA expression in the P19 mouse teratocarcinoma cell line. We used an HA tag to verify MagA protein expression and localization. We examined the response of parental and MagA-HA-expressing cells to culture in the presence and absence of an extracellular iron supplement, measuring total cellular iron content by ICP-MS. In addition, we adapted the methods previously developed by Sengupta *et al*. to measure the relaxation rates of parental P19 cells and those expressing MagA-HA using 3T MRI [6].

2.2. Methods

2.2.1 Generation of a MagA-HA Expression Construct

The tagged *MagA-HA* gene construct was kindly provided by Becky McGirr as a cloned insert within pcDNA3.1 Zeo(+), under the control of the cytomegalovirus (CMV) constitutive promoter (Life Technologies, Burlington, Canada). Using customized primers to incorporate the HA sequence (underlined in reverse MagA_HA 5′ in Table 1) and a published protocol (Goldhawk *et al.*, 2009), *MagA* was cloned by polymerase chain reaction (PCR) from *Magnetospirillum magneticum* sp. AMB-1 (ATCC, Burlington, Canada). The resultant MagA-HA PCR fragment was sub-cloned into pCR2.1-TOPO

(Life Technologies, Burlington, Canada) and shuttled into pcDNA 3.1 Zeo(+) at Kpn I/ Bam H1 (Figure 2.1).

The pcDNA3.1 Zeo(+)/MagA-HA construct expresses the HA epitope tag fused to the C-terminus of MagA. The expression of MagA-HA was confirmed by Western blot and immunocytochemistry (ICC), using commercially available antibodies (anti-HA antibody, anti-p115 antibody). A stable MagA-HA-expressing cell line was obtained using Zeocin antibiotic selection, as conferred by the BleoR resistance gene (Figure 2.1) and detailed below.

2.2.2   P19 Cell Culture, Transfection and Iron-loading

2.2.2.1   Cell of Choice

Mouse multipotent teratocarcinoma cells (P19, ATCC) were transfected with pcDNA3.1 Zeo(+)/MagA-HA and cultured under selection to obtain a clonal cell line stably-expressing MagA-HA. Cells were cultured in alpha-minimum essential medium (αMEM, Life Technologies, Burlington, Canada) and 10% fetal bovine serum (FBS) and maintained under standard cell culture conditions (37°C, 5% CO2), passaging 1:10 when the cells achieved 80-90% confluence. Whether replating or harvesting, cells were routinely dissociated using 0.25% Trypsin/0.91 mM EDTA (Life Technologies, Burlington, Canada).

2.2.2.2   Transfection Information

Transfection was performed using Lipofectamine 2000 (Life Technologies, Burlington, Canada) according to the manufacturer's instructions. Cells were 70-80% confluent on the day before transfection and replated approximately 24 hours after transfection at 1:20. Selection began 24 hours post-transfection using 200 μg Zeocin/ml medium. After approximately two weeks under selection, distinct colonies of P19 cells appeared on the plate. Several of these colonies were randomly selected and individually replated in 6–well plates for further amplification on 100 mm^2 dishes. At confluence, these clonal lines were placed in cryostorage and used to examine the expression of MagA-HA via Western blot, as described in the next section.

2.2.2.3   Iron Loading

To examine Mag-HA activity, cells were cultured in the presence or absence of iron-supplemented medium, containing 250 µM ferric nitrate (Sigma-Aldrich, Oakville, Canada). Following 7 days of iron supplementation, select plates were washed twice with PBS (phosphate buffered saline, 137mM NaCl/ 2.7 mM KCl/ 10mM HPO_4^{2-}) and returned to non-supplemented medium for an additional 24 hours of culture. At harvest, all plates of cells were washed twice with PBS and either prepared for MRI (described in Section 2.2.5), or collected for protein analysis. The latter were collected in 1 to 2 ml of ice-cold 50 mM Tris/5 mM EDTA pH 8/150 µL Complete Mini protease inhibitor cocktail (Roche Diagnostic Systems, Laval, Canada) and lysed by sonication.

Table 1 Sequences of the primers used in the generation of a *MagA-HA* construct

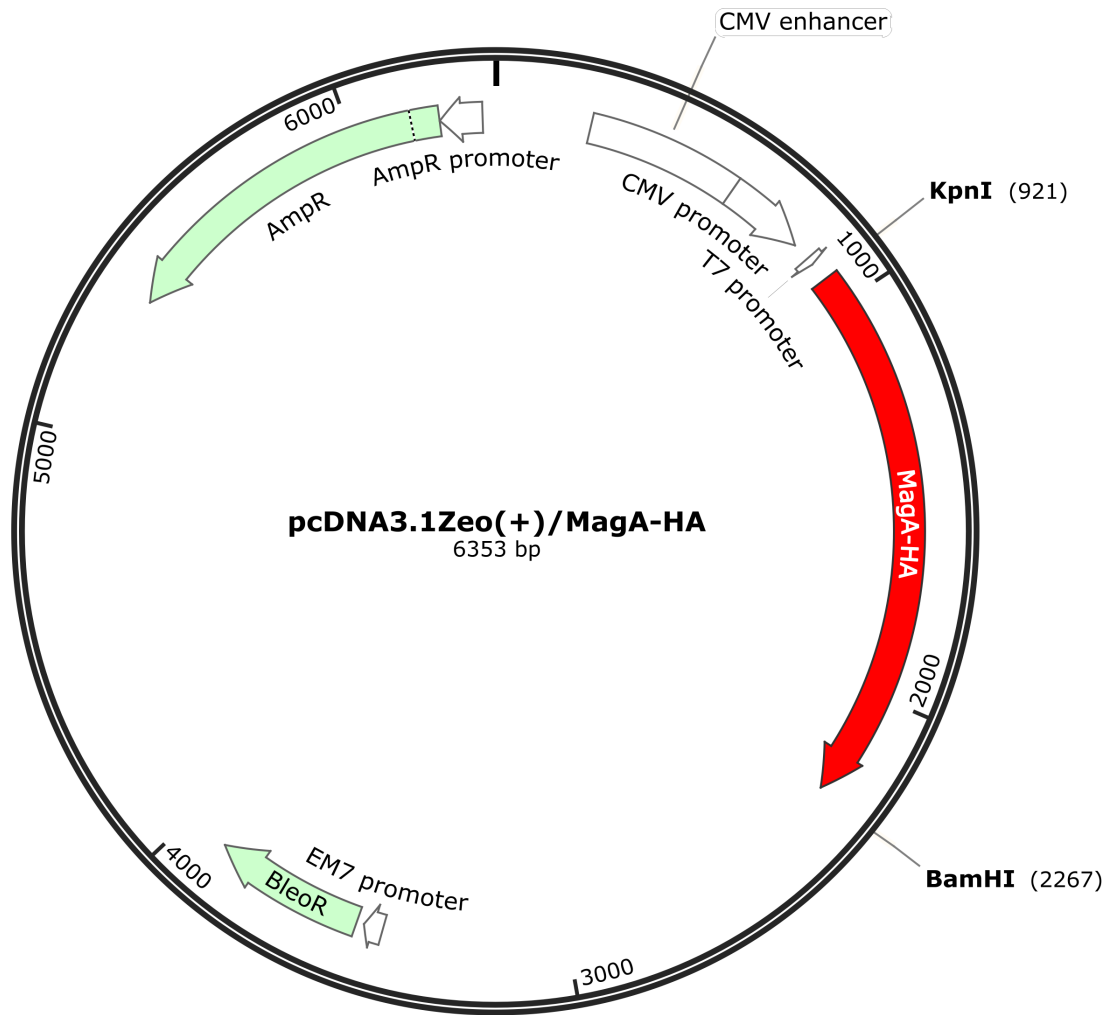| Primer Name	Sequence (5′-3′)
Forward MagA_5′	GGTACCGCCACCATGGAACTGCATCATCCCGAACTGACCTAT GCCGCCATCG
Reverse MagA-HA_3′	CCGAGACCTTAACTTAAGATAGGCATACTACACGGCCTAAT ACGCATTCCTAGGCGIX

Figure 2.1 Diagram of the plasmid vector used for transfection. The plasmid vector map of pcDNA3.1 Zeo(+) was modified to indicate the site of insertion of the *MagA-HA* DNA sequence, the relevant promoters, restriction enzyme sites used in cloning, and available antibiotic resistance genes allowing selection of clones that stably express the inserted DNA.

2.2.3   Protein Expression

2.2.3.1   Western Blot

Different clonal lines of MagA-HA-expressing P19 cells were cultured in 6-well plates until the cells reached confluence. Clonal lines of MagA-HA-expressing P19 cells (cell lines isolated as described above in Section 2.1.2) were prepared from cells cultured in T75 flasks. At harvest, they were washed twice with PBS and collected in 1 mL 50 mM Tris/5 mM EDTA pH 8/150 µL Complete Mini protease inhibitor cocktail (Roche Diagnostic Systems, Laval, Canada). Cells were lysed by sonication and protein concentration was quantified using the BCA Protein Assay Kit [8] (Thermo Fisher Scientific, Mississauga, Canada). Cellular proteins from each sample were separated by sodium dodecyl sulfate polyacrylamide gel electrophoresis (SDS PAGE, 40 µg/lane) on a precast 4-12% gradient gel (Life Technologies, Burlington, Canada) and transferred to a nitrocellulose membrane using the Original iBlot® Gel Transfer Device (Life Technologies, Burlington, Canada). Blots were blocked with 5% blotto/Tris buffered saline (TBS), 50 mM Tris-HCl pH 7.6/0.9% NaCl)/0.1% Tween 20 (TBS-T) for one hour, followed by overnight incubation at 4°C with a monoclonal antibody against HA (mouse anti-HA, 1:1,000 dilution, in 1% blotto/TBS-T). The following day, membranes were washed four times in TBS-T and incubated with secondary antibody conjugated to horseradish peroxidase (HRP) (HRP-goat anti-mouse Ig (Sigma-Aldrich, Oakville, Canada), 1:5,000 dilution, in 1% Blotto/TBS for 1 hour. Immunoblots were subsequently washed 3 times with TBS-T and once with TBS prior to development with a chemiluminescent substrate (Super Signal, Thermo Scientific). Chemiluminescence was captured using GeneSnap7.12 Software (Cambridge, England) while exposed in the Chemigenius Gel Doc (Syngene) for 5 min.

2.2.3.2   Immunocytochemistry (ICC)

Sterile glass coverslips were placed in 6-well plates and rinsed with PBS prior to seeding approximately 1 million MagA-HA-expressing P19 cells per well. At 70-80% confluence, cells were washed with PBS, fixed with 2% paraformaldehyde (PFA)/PBS for 30 min and permeabilized with 0.25% Triton X-100 (TX-100)/PBS for five min.

After washing three more times with PBS, cells were incubated with blocking buffer (10% goat serum/1% bovine serum albumin (BSA)/PBS) for one hour. Cells were subsequently incubated overnight at 4°C with goat anti-HA (Abcam, 1:100 dilution in 10% goat serum/1% bovine serum albumin (BSA)/PBS). An antibody against mouse Golgi-associated protein p115 (1:50, Transduction Laboratories, Lexington, KY) and Alexa Fluor 594-conjugated wheat germ agglutinin (WGA, 5ug/ml in 10% goat serum/1% bovine serum albumin (BSA)/PBS, Life Technologies, Burlington, Canada) were also used to visualize the Golgi Apparatus and plasma membrane, respectively. The secondary antibodies used were: Alexa Fluor 488-conjugated donkey anti-goat immunoglobulin (Ig) and Alexa Fluor 594-conjugated donkey anti-mouse Ig (Life Technologies, Burlington, Canada) respectively. After incubation with secondary antibodies for two to four hours, cover slips were mounted on glass slides using ProLong Gold Antifade Reagent (Life Technologies, Burlington, Canada). Cells were then visualized with an Olympus IX81 wide field fluorescence microscope. Image acquisition was carried out using In Vivo software. Ten optical sections per cell were collected in 0.2μm steps covering the z-axis field, using a 60 × oil immersion objective lens. Cell images were processed using a three-dimensional (3D) blind deconvolution algorithm provided in Image-Pro Plus software (Media Cybernetics, Inc., Rockville, MD, USA).

2.2.4   Trace Element (Iron) Analysis

Samples were sent to the Analytical Services Laboratory of Surface Science Western at Western University (London, Canada) for trace element analysis of iron and zinc using ICP-MS. To prepare samples, cells were cultured as described above and harvested based on the confluency of T175 flasks, a day or two before or after the actual day of MRI scanning. Cells were lysed in 1 mL 50 mM Tris-HCl pH 8/5 mM EDTA/150 μL Complete Mini protease inhibitor cocktail (Roche Diagnostic Systems, Laval, Canada) and sonicated. The total protein from lysis of these cultured cells was quantified using the bicinchoninic acid assay (BCA assay) [8]. Zinc provided a measure of cellular redox status as well as a point of comparison to amount of iron. Iron content was then normalized to quantity of total cellular protein as determined by the BCA assay. For each

individual sample group, mean and standard error of the mean (SEM) were calculated in Excel, version 14.3.8.

2.2.5   MRI of MagA-HA-expressing Cells

2.2.5.1   Phantom Preparation

Figure 2.2 depicts the spherical MRI cell phantom set-up for the measurement of relaxation rates. Approximately 40-50 million cells were placed in each well. These wells were custom-made from an NMR compatible material (Ultem, Lawson imaging Prototype Lab). The dimensions of each well are: inner diameter 4 mm and height 10 mm. Samples were centrifuged at $400 \times g$ and for 5 min to create a compact layer of cells within each well. Cell pellets were overlaid with 1% gelatin (porcine type 1, Sigma-Aldrich, Oakville, Canada)/PBS and embedded in one hemisphere of a 9cm spherical phantom filled with 4% gelatin/PBS. A spherical-shaped phantom was used to minimize macroscopic magnetic field inhomogeneity which would interfere with accurate R2' measurement. Samples consisted of either parental or MagA-expressing cells, cultured under different conditions of iron supplementation: without extra iron supplementation, with iron supplementation (250 μM ferric nitrate), and withdrawal of iron supplementation after 7 days of continuous iron supplementation. To form the spherical gelatin phantom, the empty hemisphere was filled with 4% gelatin/PBS and placed on top of the half containing cell samples. Using a layer of parafilm, air was excluded in order to avoid susceptibility artifacts at the interface [6].

2.2.5.2   Scanner and Pulse Sequences

The spherical phantom was placed in a 15-channel knee RF coil and scanned on a 3T mMR Biograph (Siemens AG, Erlangen, Germany) using previously described sequences [6]. To acquire T1-weighed images, inversion recovery spin echo sequences were used. Imaging parameters were as follows: echo time (TE) 13 ms; repetition time (TR) 4000 ms; six inversion times (TI)= 22, 200, 500, 1000, 2000, 3900ms; flip angle= 90°; total scanning time approximately 39 min. To acquire T2-weighted images, a single echo spin echo sequence and the following imaging parameters were employed: TE=13,

30, 40, 60, 80, 100, 150, 200, 300 ms; TR=2010ms; flip angle= 90°; total scanning time approximately 61 min. To acquire T2*-weighted images, a multi echo gradient echo sequence was used with: TE=6.12, 14.64, 23.16, 31.68, 40.2, 50, 60, 70, 79.9 ms; TR= 200ms; flip angle= 60°; total scanning time approximately 25 min. For all MR images, the field of view was 120×120 mm. For T1-weighted images, the volume of the voxels was 1.5×0.9×0.9 mm^3 and matrix size was 128×128. For T2- and T2*-weighted images, the voxel size was 1.5×0.6×0.6 mm^3 and matrix size was 192×192.
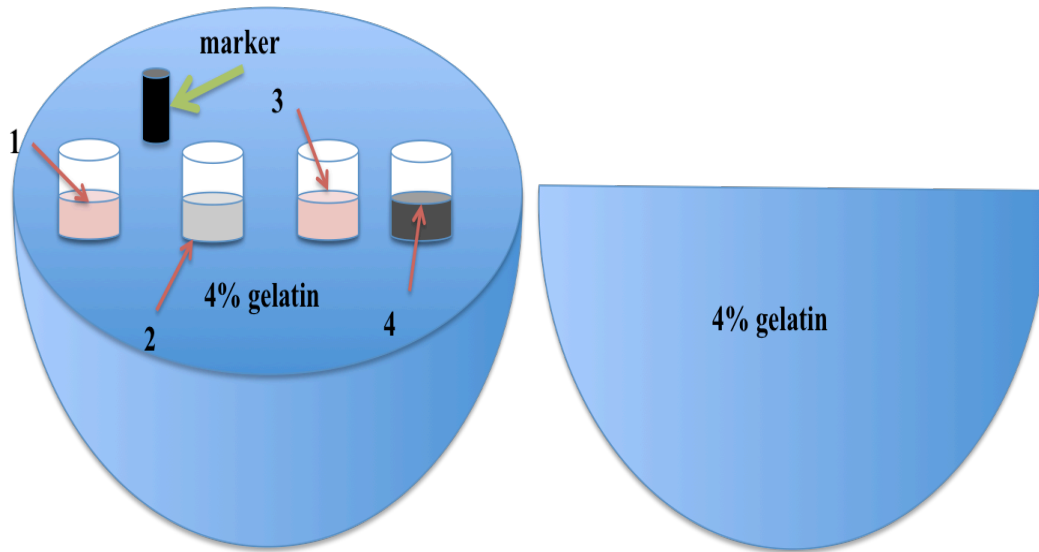
Figure 2.2 Diagram of the MRI cell phantom used for the measurement of relaxation rates. Each hemisphere of a plastic 9-cm spherical mold was filled with 4 % gelatin/PBS. Four different samples, prepared from parental and MagA-HA-expressing cells cultured in the presence (+Fe) and absence of iron supplementation, were inlaid in one of the hemispheres and arranged from left to right as follows: P19 (1), P19 + Fe (2), MagA-HA (3), MagA-HA + Fe (4)**.** A plastic marker was used to indicate orientation of the samples.

2.2.5.3   Region of Interest (ROI)

The slice thickness was 1.5 mm and selected as shown in Figure 2.3. Slices were oriented perpendicular to the sample wells to obtain a cross section through the cell layer and avoid voxels from the bottom of the well and the top gelatin layer. Specifically, a

ROI in each well was drawn using viewer code developed in Matlab 7.9.0 (R2010b), including as many voxels as possible while excluding those closest to the wall of the well (Figure 2.3 B). Overall, approximately 20 voxels were included in each ROI and average signal intensity of the ROI for each time point and relaxation rate (R2, R2* and R1) were determined with least-squares curve fitting (SigmaPlot 10.0.inc) of the mean ROI signal. Note that manual selection of ROI was done by using a graphic user interface based on Matlab 7.9.0 (R2010b) [6].
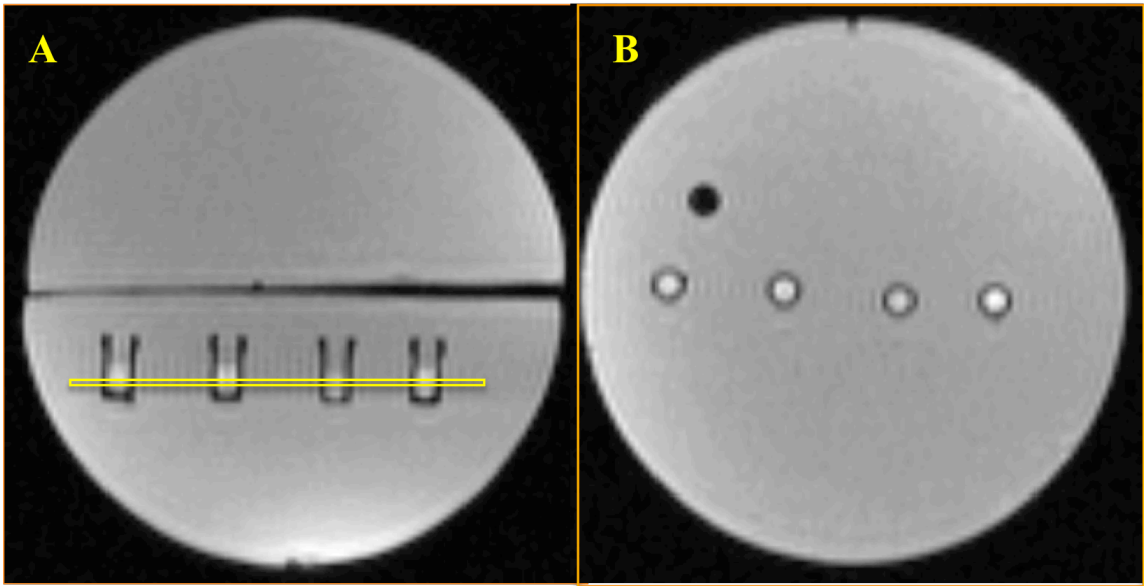
Figure 2.3 Localizer images of the spherical gelatin phantom. The images were acquired by 3T MRI. A. In the sagittal view of the phantom, a yellow box indicates the slice selected for image acquisition. B. A cross sectional view of the phantom shows the alignment of sample wells. A plastic peg (black) provides orientation.

2.2.5.4   Calculation of R1, R2, R2* and R2'

R1 decay curves were obtained using an inversion recovery pulse sequence. R1 was determined with least-squares curve fitting of the mean ROI signals using Equation 2.1.

$$S(\text{TI}) = |S_0 \cdot (1 - 2 \cdot e^{-\text{TI} \cdot \text{R1}} + e^{-TR \cdot \text{R1}})| \cdot e^{-TE/T2} \qquad (2.1)$$

R2* decay curves (average signal intensity over TEs) were obtained from the data acquired using multi-echo spin echo sequences. R2 curves were obtained from single echo spin echo pulse sequences. Sigmaplot 10.0 (Systat Software, Germany) was used to fit R2 and R2* curves with a single exponential decay equation. A two-parameter model was tested using the following equations.

$$S(TE) = S_0 e^{-TE \cdot R2} \tag{2.2a}$$

$$S(TE) = S_0 e^{-TE \cdot R2^*} \tag{2.2b}$$

Once R2* and R2 were determined, R2′ was calculated from the difference between R2* and R2 (R2′=R2*-R2). For each individual sample group, mean and SEM of relaxation rates (R1, R2*, R2 and R2′) were calculated in Excel.

2.2.6   Data Analysis

2.2.6.1   Sample Groups

To perform data analysis, samples were assigned to six groups: 1) parental P19 cells cultured in non-supplemented medium, P; 2) MagA-HA-expressing P19 cells cultured in non-supplemented medium, M; 3) iron-supplemented parental cells, P+Fe; 4) iron-supplemented, MagA-HA-expressing P19 cells, M+Fe; 5) P+Fe cells cultured for an additional 24 hours in non-supplemented medium, P 24h- Fe; and 6) M+Fe cells cultured for an additional 24 hours in non-supplemented medium, M 24h-Fe.

2.2.6.2   Statistical analysis

Two-way ANOVA was used to assess main effects and interaction between variables. All tests were two-tailed and SPSS version 20.0 was the statistical package used. Student's t-tests were used to evaluate significant differences between parental and MagA-HA-expressing P19 cells for each condition of iron supplementation. Linear regression was tested with R2' as the dependent variable and iron concentration as the independent variable. P<0.05 was set as the threshold of statistical significance.

2.3. Results

2.3.1   Generation of a Stably-expressing Cell Line

Protein lysates of both untransfected parental P19 and MagA-HA-expressing cells were collected and analyzed by Western blot. As shown in Figure 2.4A, protein lysates from parental cells (lanes 1 and 2) showed no anti-HA immunostaining. In contrast, varying degrees of HA-tagged protein are detected as a single band in transfected cells, stably expressing MagA-HA (lanes 3-6 in Figure 2.4B). The predicted molecular weight (M.W.) of MagA-HA is 46.8 KDa; the apparent M.W. of anti-HA bands is approximately 35 KDa, which is similar to results obtained in a recent report [9]. When the same blot was reprobed with an anti-β-actin antibody, a single band was stained at a M.W. of approximately 40 KDa, indicating relatively constant amounts of a common structural protein in each lane (Figure 2.4 C and D). The reported size of β-actin is 42 KDa [10, 11]. Therefore, immunoblotting confirms the presence of HA-tagged protein (Figure 2.4B), indicating the successful expression of MagA-HA in P19 cells. Comparison of panels B and D indicates a highly expressing clone in lane 3, which was selected for use in all subsequent experiments.
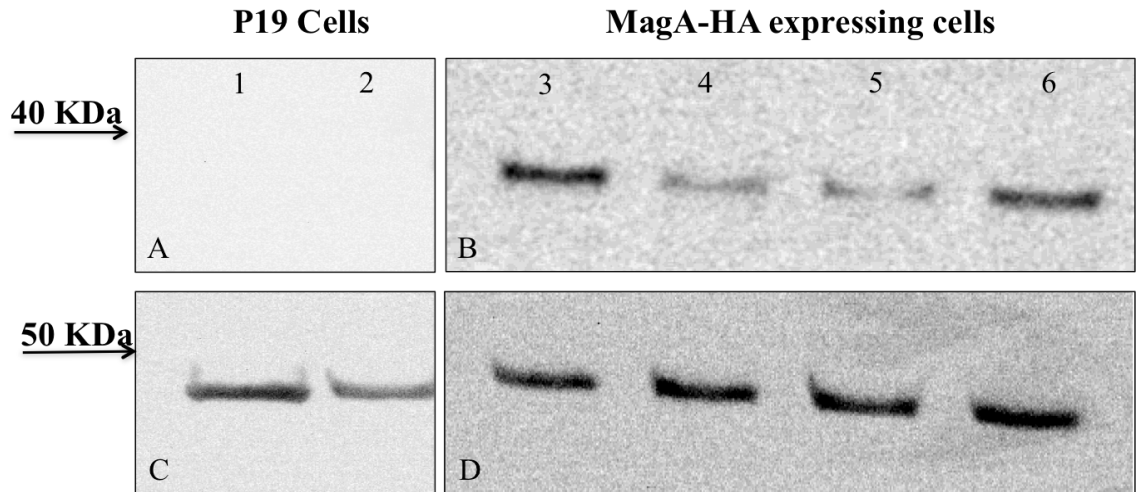
Figure 2.4 Western blots of protein extracted from P19 cells. Lanes 1-2 contain protein extracted from untransfected parental P19 cells; lanes 3-6 contain protein from MagA-HA-expressing cells. Panels A and B were probed with antibody against HA to detect MagA-HA expression. Panels C and D were probed with an antibody against beta-actin, used as a loading control. Approximate M.W. is indicated in the left margin.

2.3.2   Localization of MagA-HA in P19 Cells

Using ICC and the antibody against HA, we examined the cellular localization of MagA-HA in P19 cells. As shown in Figure 2.5A, MagA-HA is present at the plasma membrane and within the intracellular compartment. Counterstaining with fluorescently-conjugated wheat germ agglutinin provides confirmation of plasma membrane labelling (Figure 2.5 B). Merging of panels A and B (Figure 2.5 C) reveals yellow fluorescence at the plasma membrane, verifying the co-localization of MagA-HA and WGA at the plasma membrane. To address the intracellular localization of MagA-HA (Figure 2.6), cells were immuno-stained with an antibody specific to the cis-Golgi Apparatus (Figure 2.6 B). Merging of panels A and B (Figure 2.6 C) reveals intracellular yellow fluorescence indicating co-localization of MagA-HA with the cis-Golgi Apparatus membrane-associated protein p115.
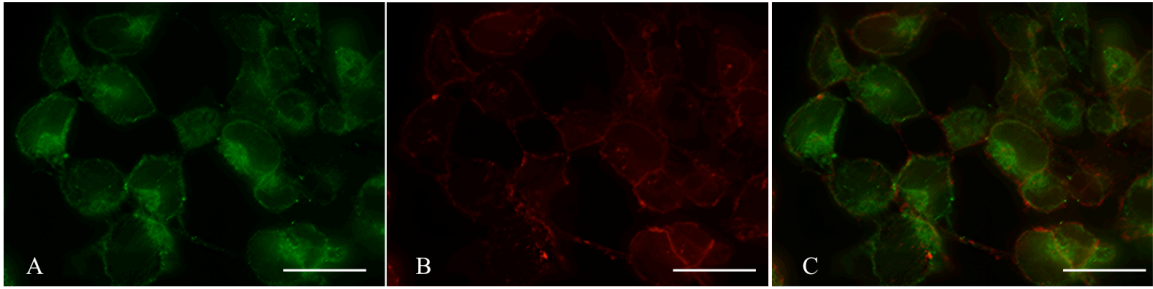
Figure 2.5 MagA-HA co-localizes with WGA at the plasma membrane. P19 cells stably expressing MagA-HA were sequentially probed with (A) primary goat anti-HA and secondary donkey anti-goat antibody conjugated to Alexa Fluor 488 (green fluorescence) and (B) Alexa Fluor 594-conjugated WGA (red fluorescence). Merging panels A and B provides yellow fluorescence (C) wherever MagA-HA and WGA co-localize in the plasma membrane. Scale bar = 15 μm.
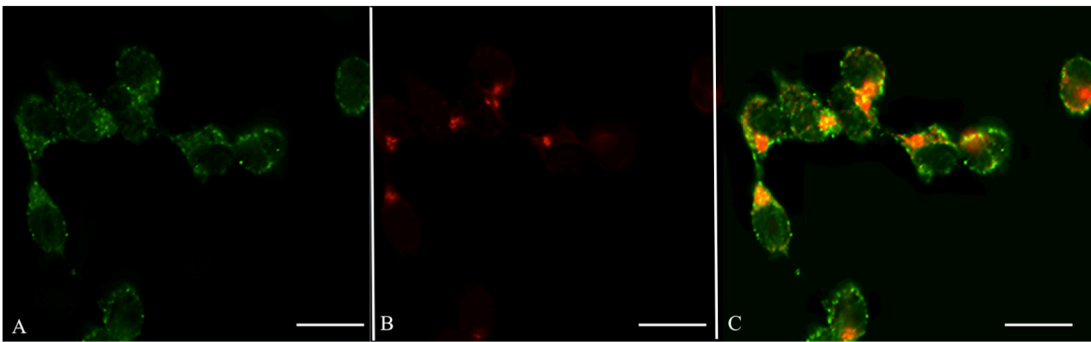
Figure 2.6 MagA-HA co-localizes with p115 expression in the Golgi Apparatus. P19 cells stably expressing MagA-HA were sequentially probed with (A) primary goat anti-HA and secondary Alexa Fluor 488 conjugated donkey anti-goat Ig (green fluorescence) and (B) primary mouse anti-p115 and secondary Alexa Fluor 594-conjugated donkey anti-mouse Ig (red fluorescence). Merging panels A and B provides yellow fluorescence (C) wherever MagA-HA and p115 are co-localized in the Golgi Apparatus. Scale bar = 15 μm.

2.3.3   Analysis of Cellular Iron in MagA-HA-expressing P19 Cells

The total cellular iron content of MagA-HA-expressing cells was examined using ICP-MS and compared to the parental control. As shown in Figure 2.7, elemental iron in both parental and MagA-HA-expressing cells is significantly increased after culture in iron-supplemented medium containing 250 μM ferric nitrate (P vs. P+Fe, $p<0.01$; M vs. M+Fe, $p< 0.01$). Under iron supplementation for 7 days, parental and MagA-HA-expressing P19 cells contain approximately 1580 ± 293 and 2100 ± 297 ng Fe/mg protein, respectively; whereas, in unsupplemented culture, parental and MagA-HA-expressing P19 cells contain approximately 48.9 ± 4.7 and 60.9 ± 12.9 ng Fe/mg protein respectively. It is noteworthy that MagA-HA expression does not cause any significant change in cellular iron content in the absence of an extracellular iron supplement, consistent with previous findings in MDA-MB-435 cells [6]. Surprisingly, however, after 7 days of iron supplementation total cellular iron content was not significantly different ($p > 0.05$) between MagA-HA-expressing P19 cells and the parental control.
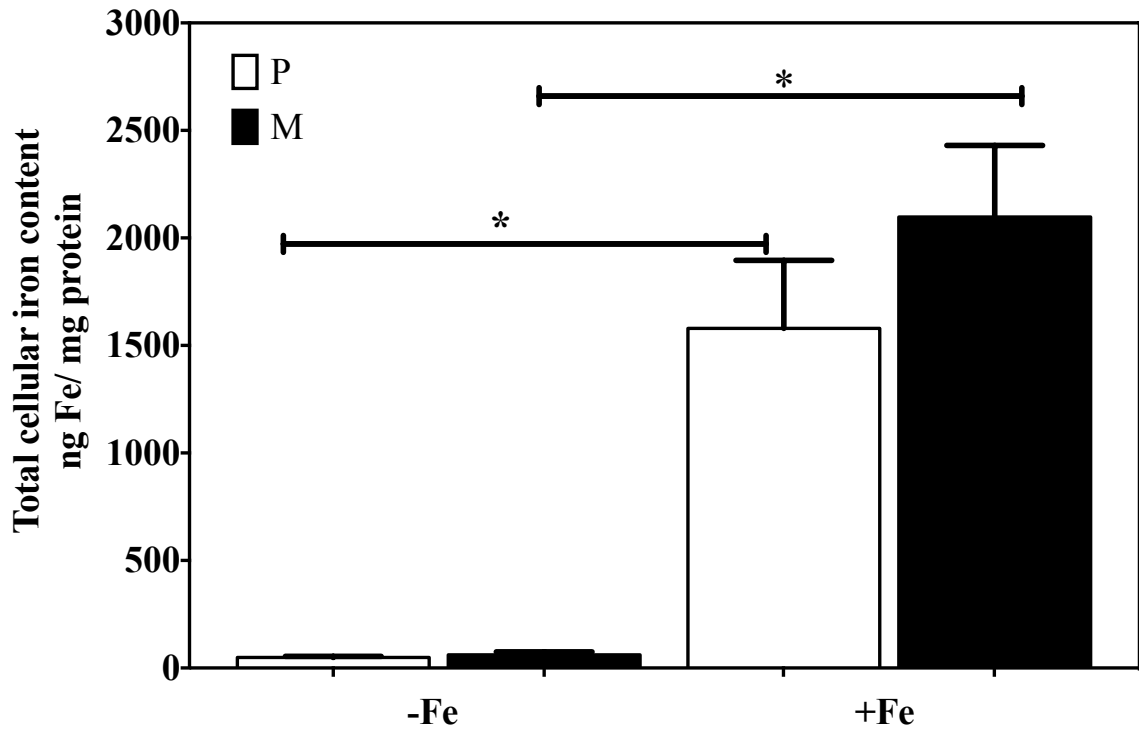
Figure 2.7 Elemental Analysis of Iron in Parental and MagA-HA-expressing P19 Cells. Total cellular iron content was analyzed by ICP-MS and normalized to total cellular protein. Cell samples were cultured at least 7 days in the presence (+Fe) and absence (-Fe) of iron supplementation (250 μM ferric nitrate). Total cellular iron content is significantly higher in both iron-supplemented cell types compared to the unsupplemented samples. Error bars are ± SEM (*, $p < 0.05$). P, parental controls; M, MagA-HA-expressing cells; P-Fe: N=6; M-Fe: N=6; P+Fe: N=8; M+Fe: N=5.

To further delineate the iron handling activities of P19 cells, their ability to retain iron after the withdrawal of the extracellular supplement was examined (Figure 2.8). Accordingly, after 7 days of iron supplementation, both parental and MagA-HA-expressing cells were returned to unsupplemented medium for an additional 24 hours of culture. In Figure 2.8, a sharp decline in iron level was observed in the parental cell type after one hour, which continued to diminish over 24 hours. However, the total cellular iron content of MagA-HA-expressing cells decreased less than the parental control and was maintained over 24 hours at a higher level than in parental P19 cells.
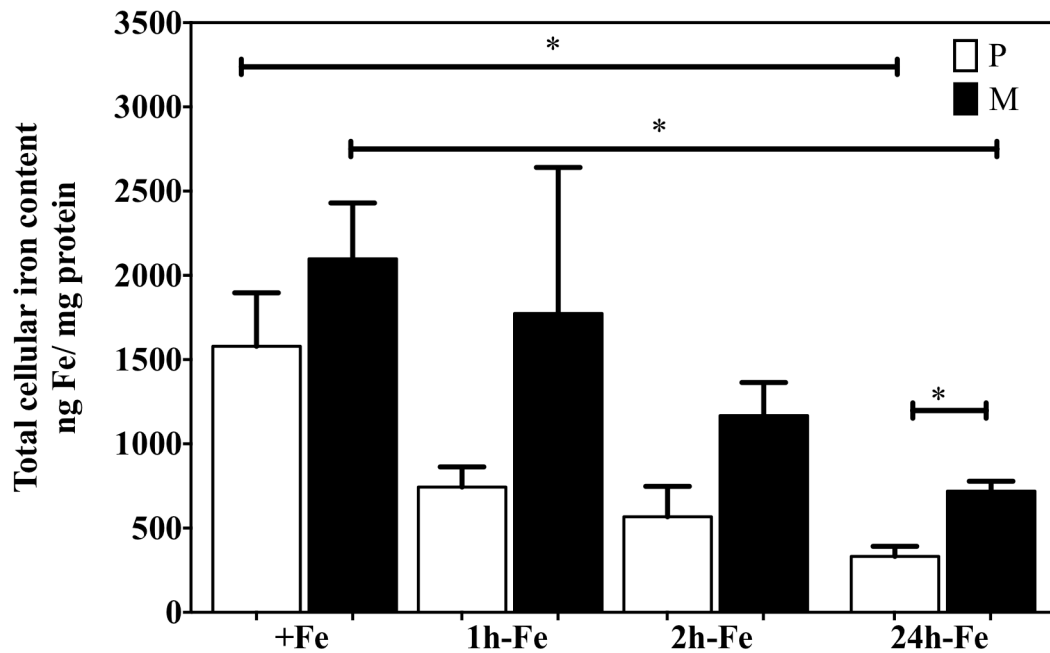
Figure 2.8 Time Course of Iron Export in P19 Cells. Both parental (P) and MagA-HA-expressing (M) P19 cells were cultured in iron-supplemented medium containing 250 μM ferric nitrate for 7 days followed by an additional 24 hours of culture in non-supplemented medium. Samples were collected for analysis by ICP-MS at 1, 2 and 24 hours after the removal of iron supplement and labeled as 1h-Fe, 2h-Fe and 24h-Fe respectively. Error bars are ± SEM (*, $p < 0.05$). P+Fe: N=8; M+Fe: N=5; 1h-Fe (P, M): N=2; 2h-Fe (P, M): N=2, 24h-Fe (P, M): N=5.

Together, Figures 2.7 and 2.8 show that untransfected and MagA-HA-expressing P19 cells have a similar capacity to incorporate iron from an extracellular supplement but different abilities to retain this iron. The parental P19 cell type demonstrates a substantial iron export activity (+Fe vs. 24h-Fe, $p < 0.01$) as do the MagA-HA-expressing P19 cells (+Fe vs. 24h-Fe, $p<0.05$). However, 24 hours after the withdrawal of iron supplement, MagA-HA-expressing cells retain approximately 719 ± 52.6 ng Fe/mg protein, which is significantly higher than the parental control (332 ± 53.6 ng Fe/mg protein, $p < 0.01$).

2.3.4   MRI of MagA-HA-expressing Cells

MR phantoms containing cell pellets from parental and MagA-HA-expressing P19 samples were scanned at 3T. Figure 2.9 shows the mean values of the longitudinal relaxation rates in parental and MagA-HA-expressing P19 cells cultured under three different conditions: -Fe, no iron supplementation; +Fe, iron supplementation for at least one week; 24h-Fe, at least a week of iron supplementation (+Fe) followed by an additional 24 hours of culture in non-supplemented medium. No significant differences in R1 measurements are observed between samples ($p > 0.05$).

Figure 2.9 Influence of iron supplementation on R1 in MagA-HA-expressing P19 cells. Longitudinal relaxation rate was determined in parental cells (P, white bars) and MagA-HA-expressing cells (M, black bars) cultured in the absence of iron supplementation (-Fe), in medium containing 250 µM ferric nitrate for 7 days (+Fe) and after withdrawal of iron from +Fe samples for 24h (24h-Fe). 3T MRI was performed as previously described [6]. There is no significant difference between P and M within a given culture condition (P-Fe vs. M-Fe and P+Fe vs. M+Fe). Error bars are ± SEM (*, $p < 0.05$). P-Fe: N=4; M-Fe: N=4; P+Fe: N=6; M+Fe: N=4; P 24h-Fe:N=2; M 24h-Fe: N=3.

When comparing the decay curves for R2 (Figure 2.10a) and R2* (Figure 2.10b) within 80 ms, R2* shows a higher signal decay rate than R2. This is consistent with a previous study in MDA-MB-435 [12]. R2* represents the total transverse relaxation rate and includes both the reversible component R2' and the irreversible component R2. In Figure 2.10, R2* decay shows a stronger difference between MagA-HA-expressing and parental cells than R2 alone.

R2 Relaxation Rates curve

R2* Relaxation Rates curve
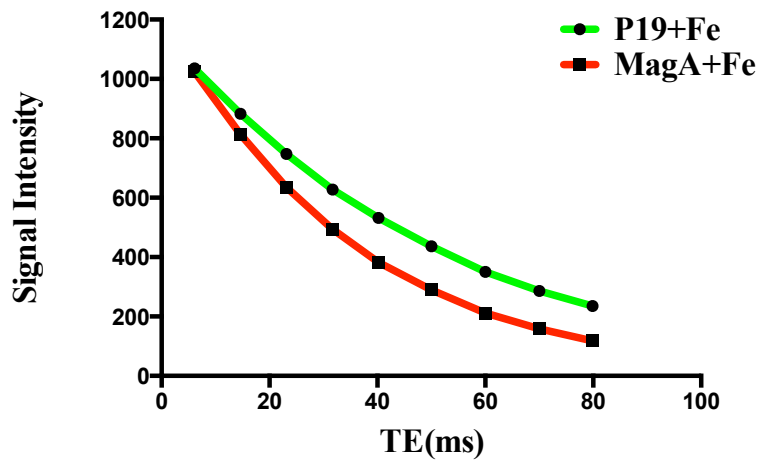
Figure 2.10 Signal Decay Curves for Transverse Relaxation. A comparison between
(a) R2 and (b) R2* relaxation curves for parental and MagA-HA-expressing cell samples,
cultured in the presence and absence of iron supplementation. In order to compare the R2
and R2* curves, only time-points before 80ms are shown in the figure. The R2* curves
show a greater difference between the MagA-HA-expressing and parental cells than the
R2 decay curves.

Previous studies show that total cellular iron content is significantly correlated to R2' [49]. In the present study, transverse relaxation rates, R2, R2* and R2′, all were notably different in both parental and MagA-HA-expressing P19 cells. For each relaxation rate, significant main effects for the iron condition were found using two-way ANOVA (Figures 2.11-2.13, $p<0.001$). The bar charts in Figure 2.11 and 2.12 show the mean values of the transverse relaxation rates of parental and MagA-HA-expressing P19 cells cultured under 3 different conditions: -Fe, +Fe and 24h-Fe. Significant differences in R2* are observed in both parental and MagA-HA-expressing P19 cells for continuously iron-supplemented and unsupplemented conditions (Figure 2.11, P-Fe vs. P+Fe and M-Fe vs. M+Fe, $p < 0.05$). Similarly, significant differences in R2 are observed in both cell types (Figure 2.12, P-Fe vs. P+Fe, $p<0.01$ and M-Fe vs. M+Fe, $p < 0.05$).
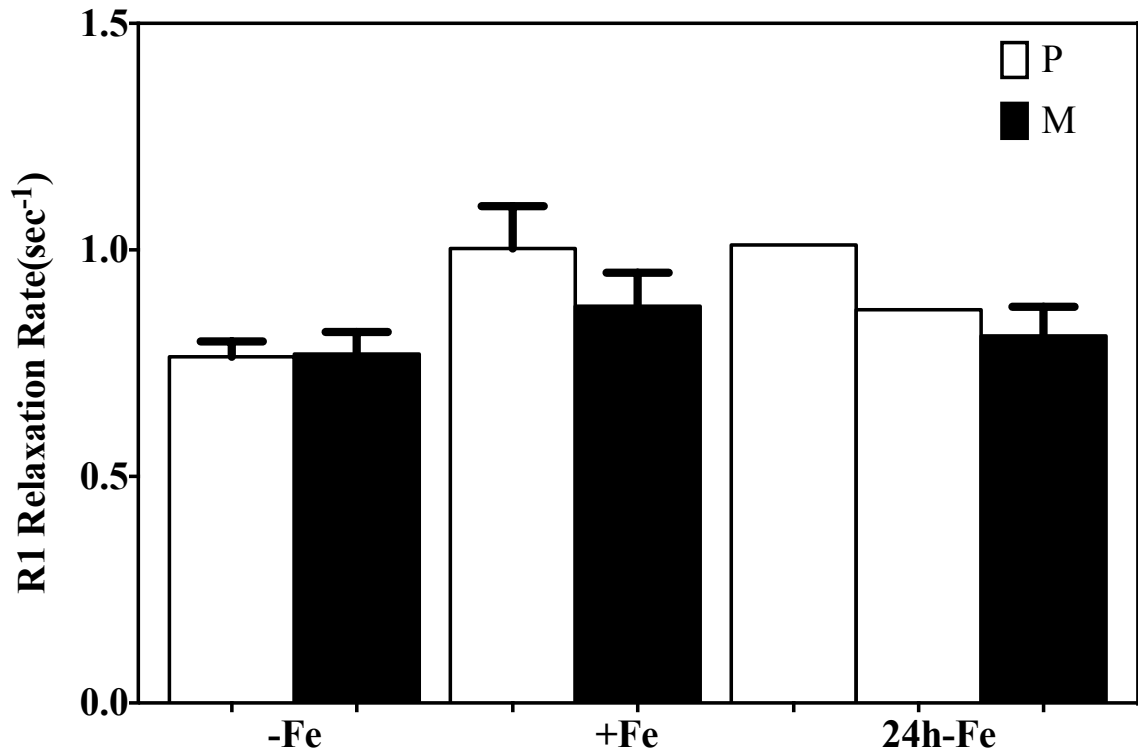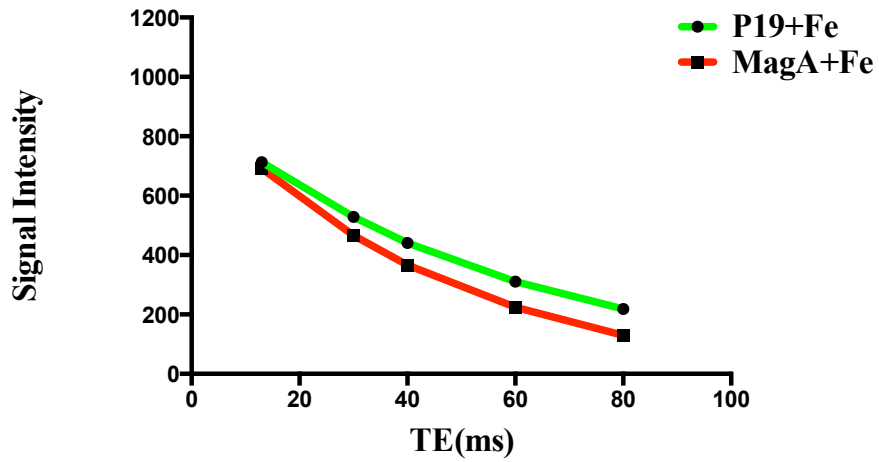
Figure 2.11 Influence of iron supplementation on R2* in MagA-HA-expressing P19 cells. R2* was determined in parental cells (P, white bars) and MagA-HA-expressing cells (M, black bars) cultured in the absence of iron supplementation (-Fe), in medium containing 250 µM ferric nitrate for 7 days (+Fe) and after withdrawal of iron from +Fe samples for 24h (24h-Fe). There is no significant difference between P and M within a given culture condition (P-Fe vs. M-Fe and P+Fe vs. M+Fe). For different conditions of iron supplementation, there is a significant difference in both P-Fe vs. P+Fe and M-Fe vs. M+Fe. Error bars are ± SEM (*, $p < 0.05$). P-Fe: N=7; M-Fe: N=4; P+Fe: N=8; M+Fe: N=4; P 24h-Fe:N=2; M 24h-Fe: N=3.

Figure 2.12 Influence of iron supplementation on R2 in MagA-HA-expressing P19 cells. R2 was determined in parental cells (P, white bars) and MagA-HA-expressing cells (M, black bars) cultured in the absence of iron supplementation (-Fe), in medium containing 250 μM ferric nitrate for 7 days (+Fe) and after withdrawal of iron from +Fe samples for 24h (24h-Fe). There is no significant difference between P and M within a given culture condition (P-Fe vs. M-Fe and P+Fe vs. M+Fe). For different conditions of iron supplementation, there is a significant difference in both P-Fe vs. P+Fe and M-Fe vs. M+Fe. Error bars are ± SEM (*, $p < 0.05$). P-Fe: N=7; M-Fe: N=4; P+Fe: N=8; M+Fe: N=4; P 24h-Fe:N=2; M 24h-Fe: N=3.

In Figure 2.13, R2' measurements were comparable between parental and MagA-HA-expressing P19 cells cultured in either the absence (-Fe) or presence (+Fe) of iron supplementation (n = 4-7). Only MagA-HA – expressing P19 cells showed significantly higher R2′ between two iron conditions (M-Fe vs. M+Fe, p< 0.05). After at least 1 week of continuous iron supplementation, parental and MagA-HA-expressing P19 cells were returned to culture for a further 24 hours in non-supplemented medium (24h-Fe). R2' measurements in this sample set show that R2' for MagA-HA-expressing cells (n = 3) is higher than parental cells (n = 2). These findings lend further support to the ICP-MS results described above, even though more experiments should be done to reach statistical significance.
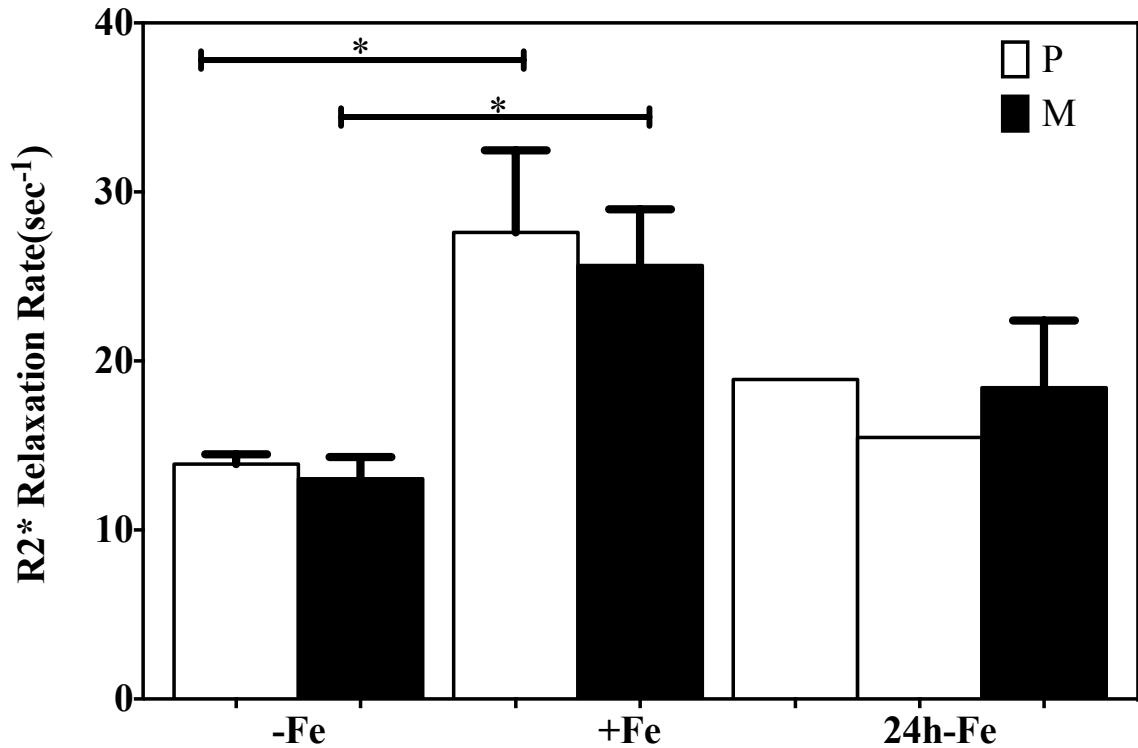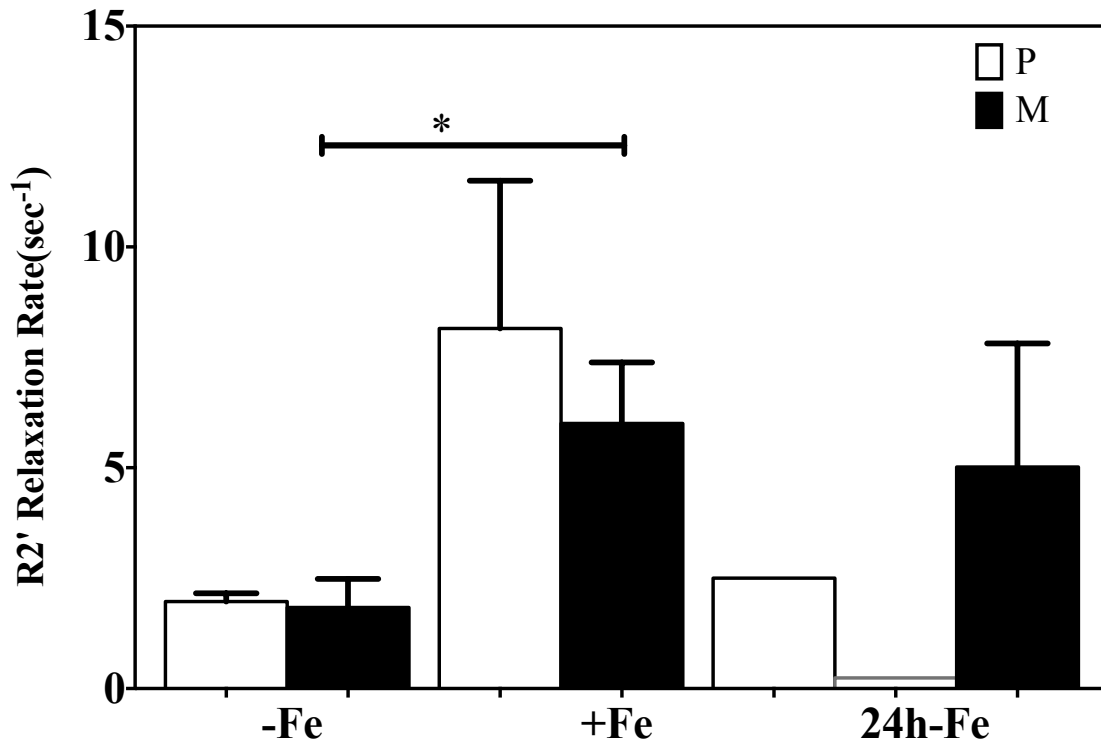
Figure 2.13 Influence of iron supplementation on R2′ in MagA-HA-expressing P19 cells. R2′ was determined in parental cells (P, white bars) and MagA-HA-expressing cells (M, black bars) cultured in the absence of iron supplementation (-Fe), in medium containing 250 μM ferric nitrate for 7 days (+Fe) and after withdrawal of iron from +Fe samples for 24h (24h-Fe). There is no significant difference between P and M within a given culture condition (P-Fe vs. M-Fe and P+Fe vs. M+Fe). For different conditions of iron supplementation, there is a significant difference in both P-Fe vs. P+Fe and M-Fe vs. M+Fe. Error bars are ± SEM (*, $p<0.05$). P-Fe: N=7; M-Fe: N=4; P+Fe: N=8; M+Fe: N=4; P 24h-Fe:N=2; M 24h-Fe: N=3.
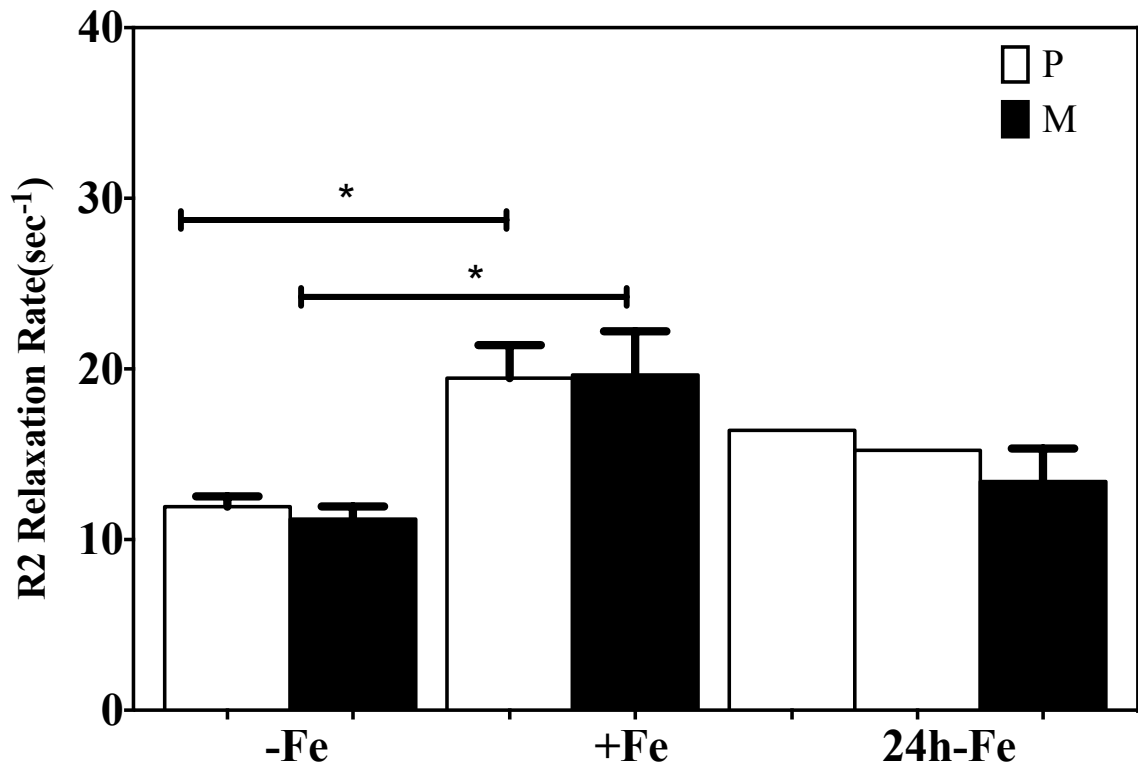
Figure 2.14 illustrates the correlation between the reversible transverse relaxation rate R2′ and total cellular iron content. Data from both parental and MagA-HA-expressing P19 cells, cultured in the presence (+Fe and 24h-Fe) and absence (-Fe) of iron supplementation, are graphed. In general, unsupplemented cultures exhibit low R2′, rising with a moderately strong correlation to the increase in total cellular iron, normalized to amount of protein. The Pearson's correlation coefficient is approximately 0.6 ($r^2 = 0.34$, n = 13, $p < 0.05$).
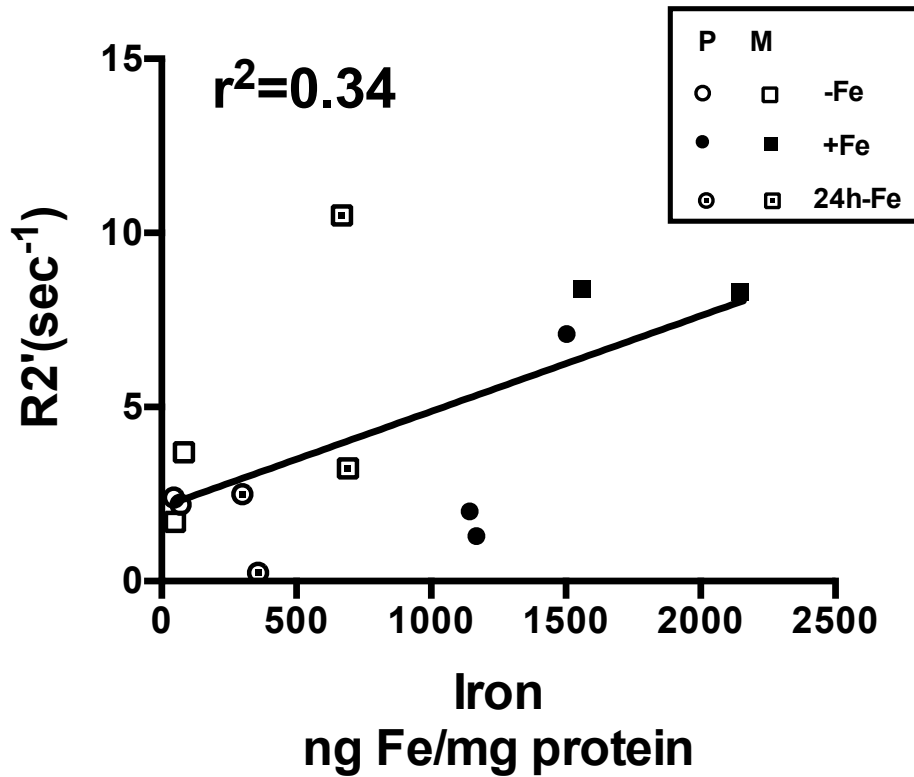
Figure 2.14 Comparison of R2′ and total cellular iron content. Samples include parental cells (P, circles) and MagA-HA-expressing cells (M, squares) cultured in the absence of iron supplementation medium (-Fe, n=2, open symbols), in medium containing 250 μM ferric nitrate for 7 days (+Fe, n=2-3, black symbols) and after withdrawal of iron for 24h (24h-Fe, n=2, dotted symbols). Relaxation rate measurements were obtained from cell samples mounted in a gelatin phantom and scanned at 3T. The plot shows a linear regression analysis of the relationship between R2′ and total cellular iron content (p < 0.05).

2.4. Discussion

In this study, we examined the expression and function of MagA-HA in undifferentiated P19 cells to extend the development of gene-based iron labelling for MRI to a model of stem cell biology. MR relaxation rates were investigated in the context of total cellular iron content in both parental and MagA-HA-expressing cells cultured under various conditions of iron supplementation (-Fe, +Fe and 24h-Fe). The results reveal new features of P19 iron biochemistry and demonstrate the potential for MagA to retain iron in P19 cells and alter MR contrast.

Protein analyses

A MagA expression construct incorporating an HA tag on the C-terminus expands the study of MagA expression to include protein analyses using immune techniques and a commercial antibody. A Western blot of MagA-HA-expressing P19 cells was used to identify a highly expressing clonal cell line (Figure 2.4). The approximate M.W. of MagA-HA is 35 KDa in agreement with a recent report using HA-tagged MagA to study the MR signal in a mouse embryonic stem cell line [9]. Although the predicted M.W. of MagA-HA is approximately 47 KDa, no post-translational processing of the N-terminal has been reported to date.

While Western blotting confirmed the expression of MagA-HA in P19 cells, ICC was conducted to examine the localization of MagA. In bacteria, MagA is a putative iron transport protein localized in the membrane compartment [13]. In mammalian P19 cells, HA-tagged protein was immuno-stained on the surface and within the intracellular compartment of MagA-HA-expressing cells. Wheat germ agglutinin is an approximately 36 kDa carbohydrate-binding protein with an affinity for sialic acid and N-acetylglucosaminyl sugar residues, which are predominately expressed on the plasma membrane of mammalian cells [14]. This lectin was used to examine the membrane localization of MagA-HA. Immunocytochemical analysis showed that MagA-HA and WGA co-localize at the plasma membrane of P19 cells (Figure 2.5). To investigate the intracellular localization of MagA-HA, we used an antibody specific for p115, a Golgi Apparatus associated protein. The Golgi Apparatus is an organelle in eukaryotic cells

responsible for sorting protein and lipid, routing them to the appropriate cellular compartment. Newly synthesized protein from the endoplasmic reticulum enters the Golgi on the cis side and leaves on the trans side facing the plasma membrane [15]. In the Golgi Apparatus, p115 is required for vesicle transport from the cis to the medial compartments [16, 17]. Thus, the Golgi Apparatus functions as a molecular assembly line in which membrane proteins may undergo extensive post-translational modification en route to their final destination in the cell. This includes processing of proteins for secretion or membrane localization [15]. Co-localization of MagA-HA and p115 in the Golgi Apparatus implies that overexpressed protein is accumulating in the Golgi vesicle(s) responsible for organizing membrane-associated protein within the cell (Figure 2.6). These results are consistent with published [7, 13] and unpublished data indicating that MagA-HA is a membrane protein.

Iron analysis

Mammalian cells display elaborate regulation of iron uptake, storage, export and distribution of intracellular iron [18]. It is a constituent of such important proteins as hemoglobin, cytochromes, oxygenases, flavoproteins, and redoxins [19]. For iron uptake, transferrin is an important extracellular antioxidant that binds iron tightly under physiological conditions so that virtually no free iron is available for the production of free radicals. The delivery of iron to cells involves receptor-mediated uptake of transferrin-bound iron [20]. Moreover, by controlling the expression of the transferrin receptor, through the interaction of iron binding proteins with iron response elements, mammalian cells regulate the amount of iron they import from the extracellular environment. This form of transferrin receptor-mediated iron uptake is present in most cell types [21]. In contrast, Ferroportin 1 (Fpn1) is the only iron exporter identified to date [18, 22-24] and its expression is largely restricted to enterocytes, macrophages and hepatocytes [25]. Once Fe(II) is exported across the basal membrane of the cell by Fpn1, the iron is oxidized by hephaestin, a multi-copper oxidase that interacts with plasma transferrin [26, 27].

Thus, iron and its careful regulation are of crucial importance to living cells. In

cultured P19 cells, the total cellular iron content increases dramatically in response to an extracellular iron supplement (Figure 2.7). Continuous culture in the presence of iron-supplemented medium results in a significant 32-fold increase ($p < 0.01$) in total cellular iron content. However, cellular iron content in parental cells also decreased abruptly with time when iron supplementation was withdrawn (Figure 2.8). Within two hours, the total cellular iron content decreased to 567 ± 181 ng iron/mg protein, approaching baseline levels by 24 hours (Figure 2.8, $p<0.05$).

While MagA-HA-expressing P19 cells exhibited a similar uptake of iron as the parental cell type after week long culture in iron-supplemented medium, the decrease in total cellular iron content, when extracellular supplementation was withdrawn, was not as great. In MagA-HA-expressing cells, total cellular iron content was more than 2-fold greater that the parental control even after withdrawal of iron supplement for 24 h (Figure 2.8; $p<0.01$). The iron export function of P19 cells is unexpected and reveals previously unrecognized iron handling abilities in this cell type. The preliminary data for parental P19 cells (white bars for 1h-Fe and 2h-Fe in Figure 2.8) indicates high ferroportin activity in addition to high transferrin receptor activity (Figure 2.7). This is similar to what is reported for M2 macrophages [28]. The ability of MagA-HA expression to retain iron in P19 cells indicates the potential of MagA activity to modulate intrinsic iron export function.

MRI analysis

While the exact mechanism of MagA function in bacterial and mammalian cells has not been fully characterized, the results in P19 agree with previous studies indicating that MagA expression increases iron incorporation in mammalian cells. With measurement of relaxation rates, we explored the potential for contrast enhancement in P19 cells by the expression of MagA-HA. Longitudinal relaxation rates (Figure 2.9) were influenced very little, by the striking increase in cellular iron and this is consistent with other publications [6, 29]. On the other hand, the transverse relaxation rates (R2* and R2, Figures 2.11 and 2.12, respectively) were strongly affected by iron supplementation in both parental and MagA-HA-expressing P19 cells.

Compared to unsupplemented cells, either parental or MagA-HA-expressing P19 cells, the transverse relaxation rates (R2* and R2) are significantly higher in iron-supplemented cells. However, there is no significant difference in these relaxation rates between MagA-HA-expressing and parental P19 cells cultured continuously in the presence of iron-supplemented medium. This is consistent with ICP-MS results, which indicate that total cellular iron content in iron-supplemented MagA-HA-expressing cells (M+Fe in Figure 2.13) is no different than the iron supplemented P19 control (P+Fe in Figure 2.13). These data are not consistent with previous studies [4, 6, 7, 9]. In other cell types, like MDA-MB-435, which downregulate transferrin receptor expression in response to iron supplementation, there is little or no increase in cellular iron content or relaxation rate in the absence of MagA expression [6]. Results in P19 suggest that the parental cell type possesses high iron import activity, which masks the activity of MagA, a putative iron transport protein from magnetotactic bacteria.

The detection of iron export activity in P19 cells prompted an investigation of relaxation rates in samples collected 24 hours after the removal of iron supplement. While there was little difference in R2 and R2* measurements at this time point, the iron specificity of R2′ measurements indicated the potential for discerning smaller differences in cellular iron content (Figure 2.13). R2′ was strongly affected by iron supplementation in MagA-HA-expressing P19 cells ($p < 0.05$) and revealed little change in MR contrast 24 hours after the withdrawal of extracellular iron. Although the sample size needs to be increased for statistical comparisons, it appears that R2′ may be a useful indicator of cellular iron content in P19 and perhaps other iron exporting cells, like macrophages. In MDA-MB-435 [6], the correlation between R2′ and total cellular iron content for MagA-expressing cells is robust (r = 0.96), with a low y-intercept indicating better iron-related specificity than R2. In P19 cells, the correlation between R2′ and total cellular iron content for parental and MagA-HA-expressing P19 cells is moderately strong (r = 0.6, Figure 2.14). We speculate that the rapid rate of iron export, particularly in the parental cell type, may be impacting this result. Using the MRI preparation protocol previously published [6], it takes about 2-3 hours to prepare cell samples for the MRI experiment. As shown in Figure 2.8, within two hours of the withdrawal of iron supplementation,

cellular iron content of parental P19 drops to approximately one third of the value measured in continuously supplemented (+Fe) controls. In this time frame, the amount of iron also decreased in MagA-HA-expressing P19 cells, by approximately 2-fold. Once more time points are examined to fully characterize the iron export activity in parental and MagA-HA-expressing P19 cells, the rate of iron export may be used to calibrate the flux in cellular iron content and its relationship to MRI measurements. Further experiments are warranted.

2.5. Conclusion

Western blots and ICC demonstrated the expression and membrane localization of MagA-HA in P19 cells. Extracellular iron supplementation of cultured cells significantly increased the total iron content in both parental and MagA-HA-expressing P19 cells, resulting in an increase in transverse relaxation rates. Withdrawal of iron supplementation revealed substantial iron export activity in parental P19 cells. MagA-HA expression attenuated this iron export function, permitting the cell to retain iron and MR contrast for a longer period of time. This is the first report of the influence of MagA expression on an iron exporting cell type.

2.6. References

1. Massoud, T. and S. Gambhir, *Molecular imaging in living subjects: seeing fundamental biological processes in a new light.* Genes Dev, 2003. **17**: p. 545-580.

2. James, M.G., SS, *A moleculae imaging primer: modalities, imaging agents, and applications.* Physiol Rev, 2012. **92**(2): p. 897-965.

3. Carlos, F., Geraldesan; Sophie, Laurent, *Classification and basic properties of contrast agents for magnetic resonance imaging.* . Contrast Media MoI. Imaging, 2009. **4**: p. 1-23.

4. Zurkiya, O.C., AW; Hu, X, *MagA is sufficient for producing magnetic nanoparticles in mammalian cells, making it an MRI reporter.* Magn Reson Med., 2008. **59**(6): p. 1225-31.

5. Goldhawk, D.R., R; Sengupta, A; Gelman, N; Prato, FS, *Using the magnetosome to model effective gene-based contrast for magnetic resonance imaging.* Wiley Interdiscip Rev Nanomed Nanobiotechnol, 2012. **4**(4): p. 378-88.

6. Sengupta, A.Q., K; Thompson, RT; Prato, FS; Gelman, N; Goldhawk, DE, *Biophysical features of MagA expression in mammalian cells: implications for MRI contrast.* Front Microbiol., 2014. **5**(29).

7. Goldhawk, D.L., C; McCreary, CR; McGirr, R; Dhanvantari, S; Thompson, RT; Figueredo, R; Koropatnick, J; Foster, P; Prato, FS, *Magnetic resonance imaging of cells overexpressing maga, an endogenous contrast agent for live cell imaging.* Mol Imaging, 2009. **8**(3): p. 129-39.

8. Smith, P.K., RI; Hermanson, GT; Mallia, AK; Gartner, FH; Provenzano, MD; Fujimoto, EK; Goeke, NM; Olson, BJ; Klenk, DC, *Measurement of protein using bicinchoninic acid.* Anal Biochem, 1985. **150**(1): p. 76-85.

9. Cho, I.M., SP; Paudyal, R; Piotrowska-Nitsche, K; Cheng, PH; Zhang, X; Mao, H; Chan, AW, *Longitudinal monitoring of stem cell grafts in vivo using magnetic resonance imaging with inducible MagA as a genetic reporter.* Theranostics, 2014. **4**(10): p. 972-89.

10. Gimona, M.V., J; Goethals, M; Herzog, M; Lando, Z; Small, JV, *Beta-actin specific monoclonal antibody.* Cell Motil Cytoskeleton, 1994. **27**(2): p. 108-16.

11. North, A.G., M; Lando, Z; Small, JV, *Actin isoform compartments in chicken gizzard smooth muscle cells.* J Cell Sci, 1994. **107**(3): p. 445-55.

12. Sengupta, A., *MRI relaxation rates: a quantative approach to track tumour cells expressing MagA.* Master Thesis, Western University, 2014.

13. Nakamura, C.B., JG; Sode, K; Matsunaga, T, *An iron-regulated gene, MagA, encoding an iron transport protein of Magnetospirillum sp. strain AMB-1.* J Biol Chem, 1995. **270**(47): p. 28392-6.

14. Wright, C., *Structural comparison of the two distinct sugar binding sites in wheat germ agglutinin isolectin II.* J Mol Biol, 1984. **178**(1): p. 91-104.

15. Tamaki, H.Y., S, *The stack of the golgi apparatus.* Arch Histol Cytol, 2002. **65**(3): p. 209-18.

16. Barroso, M.N., DS; Sztul, E, *Transcytosis-associated protein (TAP)/p115 is a general fusion factor required for binding of vesicles to acceptor membranes.* Proc Natl Acad Sci U S A, 1995. **92**(2): p. 527-31.

17. Waters, M.C., DO; Rothman, JE, *A novel 115-kD peripheral membrane protein is required for intercisternal transport in the Golgi stack.* J Cell Biol, 1992. **118**(5): p. 1015-26.

18. Hentze, M.M., MU; Andrews, NC, *Balancing acts: molecular control of mammalian iron metabolism.* Cell, 2004. **117**(3): p. 285-97.

19. MacKenzie, E.I., K; Tsuji, Y, *Intracellular iron transport and storage: from molecular mechanisms to health implications.* Antioxid Redox Signal, 2008. **10**(6): p. 997-1030.

20. Cheng, Y.Z., O; Aisen, P; Harrison, SC; Walz, T, *Structure of the human transferrin receptor-transferrin complex.* Cell, 2008. **116**(4): p. 565-76.

21. Hentze, M.M., MU; Galy, B; Camaschella, C, *Two to tango: regulation of Mammalian iron metabolism.* Cell, 2010. **142**(1): p. 24-38.

22. Abboud, S.H., DJ, *A novel mammalian iron-regulated protein involved in intracellular iron metabolism.* J Biol Chem, 2000. **275**(26): p. 19906-12.

23. Donovan, A.B., A; Zhou, Y; Shepard, J; Pratt ,SJ; Moynihan, J; Paw, BH; Drejer, A; Barut, B; Zapata, A; Law, TC; Brugnara, C; Lux, SE; Pinkus, GS; Pinkus, JL; Kingsley, PD; Palis, J; Fleming, MD; Andrews, NC; Zon, LI, *Positional cloning of zebrafish ferroportin 1 identifies a conserved vertebrate iron exporter.* Nature, 2000. **403**(6771): p. 776-81.

24. McKie, A.M., P; Rolfs, A; Brennan, K; Wehr, K; Barrow, D; Miret, S; Bomford, A; Peters, TJ; Farzaneh, F; Hediger, MA; Hentze, MW; Simpson, RJ, *A novel duodenal iron-regulator transporter, IREG1, implicated in the basolateral transfer of iron to the circulation.* Mol Cell, 2000. **5**(2): p. 299-309.

25. Ganz, T.N., E, *Hepcidin and iron homeostasis.* Biochim Biophys Acta, 2012. **1823**(9): p. 1434-43.

26.   Vulpe, C.K., YM; Murphy, TL; Cowley, L; Askwith, C; Libina, N; Gitschier, J; Anderson, GJ, *Hephaestin, a ceruloplasmin homologue implicated in intestinal iron transport, is defective in the sla mouse.* Nat Genet, 1999. **21**(2): p. 195-9.

27.   McKie, A.B., DJ, *The SLC40 basolateral iron transport family (IREG1/ferroportin/MTP1).* Pflugers Arch, 2004. **447**(5): p. 801-6.

28.   Corna, G.C., L; Pignatti, E; Castiglioni, A; Tagliafico, E; Bosurgi, L; Campanella, A; Brunelli, S; Manfredi, AA; Apostoli, P; Silvestri, L; Camaschella, C; Rovere-Querini, P, *Polarization dictates iron handling by inflammatory and alternatively activated macrophages.* Haematologica, 2010. **95**(11): p. 1814-22.

29.   Na, H.S., IC; Hyeon, T *Inorganic nanoparticles for MRI contrast agents.* Adv Mater, 2009. **21**(21): p. 2133-48.

Chapter 3

3.1   Summary

This thesis describes the successful expression of *MagA*, a gene from the magnetotactic bacterium species AMB-1, in undifferentiated P19 mouse embryonal carcinoma cells and generation of a stable MagA-HA-expressing clonal cell line. Our study reports the cellular location of MagA-HA using immunocytochemistry, the response of MagA-HA-expressing cells to extracellular iron supplementation using mass spectrometry and their magnetic properties using MR relaxation rates. A comparison to parental P19 cells reveals (1) pronounced iron uptake and export functions not previously described in this model of stem cell behaviour, (2) the influence of MagA on mammalian iron export and (3) the ability of MagA-HA expression to provide MR contrast in an iron-exporting cell type.

3.2   Future Directions

P19 cells are a mouse teratocarcinoma, multipotent stem cell line, which can be chemically induced to differentiate into different cell lineages. Previous studies have shown that P19 cells can be differentiated down the mesodermal lineage using dimethyl sulfoxide (DMSO) [1]. Using this procedure, successfully differentiated P19 cells display a beating cardiac muscle cell phenotype in culture, with appropriate immunocytochemical staining of cardiac biomarkers [2]. In preliminary experiments, differentiated MagA-HA-expressing P19 cells also exhibited a beating cardiac muscle cell phenotype. However, further immunocytochemical experiments need to be done to show that the expression of MagA-HA is fully compatible with cardiac differentiation.

Magnetosomes, the membrane bound crystals of magnetite or greigite, permit magnetotactic bacteria to navigate along the geomagnetic field. In order to accumulate the large quantities of iron needed for magnetosome production, pathways for active iron uptake into the cell, and more specifically the magnetosomal compartment, are very important. It is still not entirely clear which genes are involved in the process of

magnetosome iron transport. Early genetic and biochemical studies indicated that MagA might be involved in magnetosomal iron uptake. This led to development of MagA as a genetic MRI reporter for non-invasive cell tracking *in vivo*. However, the gene for MagA is not located within the magnetosome genomic island [3], which is assumed to contain the essential genes necessary for the formation of magnetosomes in bacteria [4]. MmsF, for example, is one of the genes encoded in the MAI region. Previous study indicates that MmsF plays an important role in biomineralization of mature magnetite crystals, which might make it suitable for study if MmsF-expressing P19 cells can increase cellular relaxation rates.

During the time course of iron export in P19 cells (Figure 2.8), we saw a high iron export activity in both parental and MagA-HA-expressing cells. More experiments detailing the time course of iron export after withdrawal of iron supplementation are needed in order to fully understand the influence of iron export. Zurkiya *et al*. showed that iron uptake in 2B5 cells changes with time and doxycycline induction of MagA expression [5]. An appreciation of the pattern of iron export in P19 cells may shed some light on the variability between total cellular iron content and R2′. Preparation of the MR phantom required large scale cell culture and in the time it took to harvest the samples more iron may have been exported from the cells, potentially affecting the correlation of cellular iron content and MR relaxation rates.

As shown in the appendix B, uncertainties in relaxation rate measurements are well within an acceptable range, and do not explain the variability in MRI measurements. However, as shown in Figure 2.8, iron content changes dramatically within hours of withdrawal of iron supplementation, which suggests that iron content may vary during the hours needed to prepare the MRI samples. As discussed above, iron homeostasis is a tightly regulated process. The only recognized iron export protein in mammalian cells is Fpn1, which is mainly found in enterocytes, macrophages and hepatocytes. Hepcidin is an important regulator of iron homeostasis: degrading the iron exporter Fpn 1 and thus influencing the exporting ability of cells. This has been substantiated by studies showing that increased hepcidin concentrations in plasma can cause anemia. On the other hand,

deficiency of hepcidin can cause iron overload [6]. In P19 cells, the addition of hepcidin to culture medium prior to cell harvest might improve the relationship between total iron content and R2′ by interrupting any residual iron export occurring during the hours of cell phantom preparation.

In MDA-MB-435 cells [7], there is a strong correlation between the reversible transverse relaxation rate, R2′ and total cellular iron content (r = 0.96). However, there is not as strong a correlation between R2′ and total cellular iron content in P19 cells (Figure 2.14); the Pearson's correlation coefficient, 0.6 (r^2 = 0.34, n = 13), implies a moderate correlation and suggests that while 34% of the variance in R2′ is explained by a change in total cellular iron content, other factors are important. In addition to rate of iron export, discussed above, further analysis, for example using an independent t test on both parental and MagA-HA-expressing samples collected at 24h - Fe, will require additional experiments.

3.3   References

1.   Jasmin, S., DC; Campos de Carvalho, AC; Mendez-Otero, R, *Chemical induction of cardiac differentiation in p19 embryonal carcinoma stem cells.* Stem Cells Dev, 2010. **19**(3): p. 403-12.

2.   Douglas, G.M., R; Charlton, CL; Kagan, DB; Hoffman, LM; Luyt, LG; Dhanvantari, S, *Characterization of a far-red analog of ghrelin for imaging GHS-R in P19-derived cardiomyocytes.* Peptides, 2014. **54**: p. 81-8.

3.   Uebe, R.H., V; Schüler, D, *The MagA protein of Magnetospirilla is not involved in bacterial magnetite biomineralization.* J Bacteriol, 2012. **194**(5): p. 1018-23.

4.   Nudelman, H.Z., R, *Structure prediction of magnetosome-associated proteins.* Front Microbiol, 2014. **5**(9): p. 1-17.

5.   Zurkiya, O.C., AW; Hu, X, *MagA is sufficient for producing magnetic nanoparticles in mammalian cells, making it an MRI reporter.* Magn Reson Med., 2008. **59**(6): p. 1225-31.

6.   Ganz, T.N., E, *Hepcidin and iron homeostasis.* Biochim Biophys Acta, 2012. **1823**(9): p. 1434-43.

7.   Sengupta, A., *MRI relaxation rates: a quantative approach to track tumour cells expressing MagA.* Master Thesis, Western University, 2014.

Appendix A: MagA-HA sequence

917   GGTACCGCCACCATGGAACTGCATCATCCCGAACTGACCTATGCCGCCATCG

TCGCCCTGGCCGCCGTGCTGTGCGGCGGGATGATGACGCGCCTGAAGCAGCC

GGCCGTCGTCGGCTACATCCTGGCGGGGGTGGTGCTGGGACCCAGCGGCTTC

GGGCTGGTGAGCAACCGCGACGCCGTGGCCACCCTGGCCGAGTTCGGCGTGC

TGATGCTGCTGTTCGTCATCGGCATGAAGCTGGACATCATCCGCTTTCTCGAA

GTGTGGAAGACGGCCATCTTCACCACGGTTCTGCAGATCGCCGGCAGCGTGG

GCACGGCCCTGCTGCTGCGTCACGGCCTGGGCTGGAGCCTGGGGCTGGCGGT

GGTGCTGGGCTGTGCCGTGGCGGTGTCGTCCACCGCCGTAGTGATCAAGGTG

CTGGAATCCTCGGACGAGCTGGACACGCCGGTCGGCCGCACCACCCTTGGCA

TCCTGATCGCCCAGGACATGGCGGTGGTGCCCATGATGCTGGTGCTGGAATC

CTTCGAGACCAAGGCGCTGCTGCCCGCCGACATGGCCCGGGTGGTGCTGTCG

GTGCTGTTCCTGGTGCTGCTGTTCTGGTGGCTGTCCAAGCGCCGCATCGACCT

GCCGATCACCGCCCGGCTTTCCCGCGATTCTGACCTTGCCACCCTGTCGACCC

TGGCCTGGTGTTTCGGCACCGCCGCCATCTCCGGCGTGCTGGACTTGTCGCCG

GCCTATGGCGCCTTCCTGGGCGGCGTGGTGCTGGGCAATTCCGCCCAGCGCG

ACATGCTGTTGAAGCGTGCCCAGCCCATCGGCAGCGTGCTGCTGATGGTGTTC

TTCCTGTCCATCGGGCTGCTGCTCGACTTCAAGTTCATCTGGAAGAATCTGGG

CACCGTTCTCACCCTGCTGGCCATGGTGACCCTGTTCAAGACGGCGCTGAAC

GTCACGGCGCTGCGCCTGGCGCGGCAGGACTGGCCCAGCGCCTTCCTGGCCG

GCGTGGCCCTGGCCCAGATCGGCGAGTTCTCGTTCCTGCTGGCCGAGACCGG

CAAGGCGGTCAAGCTGATCAGCGCCCAGGAGACCAAGCTGGTGGTGGCGGT

CACCGTGCTGTCCCTGGTGCTGTCGCCGTTCTGGCTGTTCACCATGCGGCGCA

TGCACCGGGTGGCGGCGGTGCATGTCCATTCGTTCCGCGATCTGGTCACGCG

GCTGTATGGCGACGAGGCCCGCGCTTTCGCCCGCACCGCGCGGCGGGCCCGT

GTGCTGGTGCGGCGTGGTTCCTGGAGGGATGACCCCAATGCCGGACCTGGCT

CTGGAATTGAATT**TATCCTATGATGTGCCGGATTATGCG**TAAGGATCC   2272

Figure A. MagA-HA sequence in pcDNA3.1 Zeo(+)/MagA-HA. The sequence is from the 5' insertion site to the stop codon following the HA tag. The numbers indicate the location of the sequence in the plasmid. The HA tag is in bold, and MagA is underlined. The start and stop codons are shaded. Unique restriction sites within this region of the plasmid are identified.

Appendix B: Raw data of relaxation rates for parental and MagA-HA expressing P19 cells in different media condition

R1 Relaxation Rates (S^{-1})							AVG	SD	SEM
P	0.70	0.90	0.70	0.70			0.75	0.10	0.05
M	0.70	0.90	0.80	0.70			0.8	0.10	0.05
P+Fe	1.00	1.00	1.20	1.20	0.80	0.90	1.1	0.12	0.05
M+Fe	1.10	1.00	0.70	0.80			0.9	0.18	0.09
P 24h-Fe	1.00	0.90							
M 24h-Fe	0.90	0.70	0.90				0.8	0.12	0.07
Uncertainty of R1 (S^{-1})									
P	0.03	0.03	0.03	0.03					
M	0.03	0.04	0.03	0.02					
P+Fe	0.60	0.06	0.09	0.05	0.03	0.06			
M+Fe	0.07	0.07	0.05	0.03					
P 24h-Fe	0.10	0.06							
M 24h-Fe	0.07	0.03	0.08						

R2* Relaxation Rates (S^{-1})								AVG	SD	SEM
P	13.50	14.10	11.10	12.30	14.10	15.30	15.40		13.69	1.56	0.59
M	10.60	12.10	16.20	12.90					12.95	2.37	1.18
P+Fe	19.00	19.90	28.00	46.90	13.80	49.40	19.50	23.00	27.44	13.41	4.74
M+Fe	28.90	27.10	31.00	15.90					25.73	6.74	3.37
P 24h-Fe	18.90	16.70									
M 24h-Fe	26.10	15.40	13.50						18.33	6.79	3.92
Uncertainty of R2* (S^{-1})											
P	0.01	0.07	0.03	0.07	✖	0.06	0.20				
M	0.03	0.10	0.05	0.10							
P+Fe	0.10	0.20	0.30	0.80	0.08	0.90	✖	0.10			
M+Fe	0.30	0.40	0.40	0.20							
P 24h-Fe	0.10	0.10									
M 24h-Fe	0.10	0.20	0.30								

R2 Relaxation Rates (S^{-1})								AVG	SD	SEM
P	11.50	11.90	9.40	10.50	12.40	13.60	12.50		11.69	1.39	0.52
M	9.60	10.40	12.70	11.90					11.15	1.41	0.70
P+Fe	17.70	17.80	20.90	31.30	11.60	30.20	16.10	18.00	20.45	6.87	2.43
M+Fe	24.20	18.80	22.30	12.90					21.77	4.97	2.48
P 24h-Fe	16.40	15.20									
M 24h-Fe	15.60	14.70	9.20						13.17	3.46	2.00
Uncertainty of R2 (S^{-1})										
P	0.30	0.20	0.10	0.40	✖	0.30	0.20				
M	0.20	0.08	0.20	0.20							
P+Fe	0.30	0.30	0.50	0.60	0.20	1.10	✖	0.50			
M+Fe	0.50	0.40	0.60	0.30							
P 24h-Fe	0.20	0.20									
M 24h-Fe	0.20	0.20	0.20								

R2′ Relaxation Rates (S^{-1})								AVG	SD	SEM
P	2.00	2.20	1.70	1.80	1.70	1.70	2.90		2.00	0.44	0.17
M	1.00	1.70	3.50	1.00					1.80	1.18	0.59
P+Fe	1.30	2.10	7.10	15.60	2.20	19.20	3.40	5.00	6.99	6.75	2.39
M+Fe	4.70	8.30	8.70	3.00					6.18	2.78	
P 24h-Fe	2.50	1.50									
M 24h-Fe	10.50	0.70	4.30						5.17	4.96	2.86
Uncertainty of R2′ (S^{-1})										
P	0.30	0.21	0.10	0.41	✖	0.31	0.28				
M	0.20	0.13	0.21	0.22							
P+Fe	0.28	0.35	0.58	1.00	0.22	1.42	✖	0.51			
M+Fe	0.58	0.57	0.72	0.36							
P 24h-Fe	0.22	0.22									
M 24h-Fe	0.22	0.28	0.36								

Uncertainties correspond to each data point. ✖: , Uncertainty information was lost due to computer malfunction. AVE: average; SD: standard deviation; SEM: standard error of the mean.

Curriculum Vitae

Linshan Liu

EDUCATION

09/12 - present **M.Sc. Candidate**

Department of Medical Biophysics

The University of Western Ontario, London , Ontario, Canada

Supervisors: Drs. Donna Goldhawk and Lisa Hoffman

09/08-07/12 **B.Sc. (Honours)**

Department of Physics Science

Qufu Normal University, QuFu, ShanDong, China

Professional Skills

Foreign Languages: Chinese (advanced speaking and intermediate writing); English (advanced speaking and intermediate writing)

Main Courses

Electromagnetics, Atomic Physics, Electrodynamics, Quantum Mechanics , Medical Imaging, NMR, Molecular Imaging, MRI Physics, Scientific Communication

SCHOLARSHIPS AND AWARDS

2013-2015 Scholarship from the CIHR Strategic

Training Program in Vascular Research

2012-2013 Western Graduate Research Scholarship

The University of Western Ontario

2012 Provincial Outstanding Graduates

Qufu Normal University, Qufu, ShanDong, China

Related Work Experience

2011-2012   Tutor in Math and Physics ,China

Publications:

Bondoc, A., Detombe, S., Dunmore-Buyze, J., Gutpell, K., **Liu, L.**, Kaszuba, A. , McGirr, R., Hadway, J., Drangova, M., & L. Hoffman. Application of three-dimensional echocardiography and gated micro-CT to assess cardiomyopathy in a mouse model of Duchenne muscular dystrophy. Ultrasound in Medicine & Biology (2014) - [Accepted]

Conference Abstracts:

Liu L, Gelman N, McGirr R, Thompson RT, Prato FS, Hoffman L and Goldhawk DE (2015) Comparison of Iron-related MR Susceptibility and Transverse Relaxation Rates in the P19 Cell Mode. International Society for Magnetic Resonance in Medicine (ISMRM). Abstract 5022. Toronto, Canada

Liu L, McGirr R, Thompson RT, Prato FS, Goldhawk DE, and Hoffman L, (2014) Non-Invasive Targeting of Cardiomyocyte-Like Cells for the Treatment of Duchenne Muscular Dystrophy-Related Cardiomyopathy using MRI/PET. London Health Research Day, London, Canada

Liu L, McGirr R, Gelman N ,Thompson RT, Prato FS, Hoffman L and Goldhawk DE (2014) Non-Invasive Targeting of Cardiomyocyte-Like Cells for the Treatment of Duchenne Muscular Dystrophy-Related Cardiomyopathy using MRI/PET (ImNO). Abstract accepted. Toronto, Canada.

Liu L, Thompson RT, Prato FS, Goldhawk DE and Hoffman L (2014) Non-Invasive Targeting Myocardial Progenitor Cells for the Treatment of Duchenne Muscular Dystrophy-Related   Cardiomyopathy using MRI/PET. Abstract accepted. Canadian Connective Tissue Society London, Canada

Liu L, McGirr R, Thompson RT, Prato FS, Goldhawk DE, and Hoffman L (2014) Targeting P19-derived Cardiomyocytes for Treatment of Duchenne Muscular Dystrophy-Related Cardiomyopathy using MRI. Abstract accepted. Cell Tracking Symposium. London, Canada

 Liu L, Thompson RT, Prato FS, Goldhawk DE and Hoffman L(2013) Non-Invasive Targeting Myocardial Progenitor Cells for the Treatment of Duchenne Muscular Dystrophy-Related Cardiomyopathy using MRI/PET(Till & McCulloch Meetings). Abstract 161. Banff, Canada.

Liu L , Goldhawk, D., & Hoffman, L. (2013) MR Reporter Gene Expression to Non-invasively Target Cardiac Stem Cells for the Treatment of Duchenne Muscular Dystrophy-Related Cardiomyopathy. London Health Research Day, London, Canada

Bondoc, A., **Liu, L.**, Gutpell, K., McGirr, R., & L. Hoffman. Imaging myocardial progenitor cells to treat Duchenne muscular dystrophy-related cardiomyopathy. London Health Research Day London, Ontario, March 18, 2014.

Bondoc, A., **Liu, L.**, Gutpell, K., McGirr, R., & L. Hoffman. Imaging myocardial progenitor cells to treat Duchenne muscular dystrophy-related cardiomyopathy. 2014 Cell Tracking Symposium London, Ontario, June 20, 2014.

Bondoc, A., Detombe, S., Dunmore-Buyze, J., Gutpell, K., **Liu, L.**, Kaszuba, A. , McGirr, R., Hadway, J., Drangova, M., & L. Hoffman. Application of 3D echocardiography and

gated micro-CT to assess cardiomyopathy in a Duchenne muscular dystrophy mouse model. ImNO 2014 Toronto, Ontario, March 24-25, 2014.

Bondoc, A., **Liu, L**., Gutpell, K., McGirr, R., & L. Hoffman. Imaging myocardial progenitor cells to treat Duchenne muscular dystrophy-related cardiomyopathy. 2014 CCTC London, Ontario, June 8-10, 2014

Bondoc, A., **Liu, L**., Gutpell, K., McGirr, R., & L. Hoffman. Imaging myocardial progenitor cells to treat Duchenne muscular dystrophy related cardiomyopathy. 2013 AGM StemCell Network of Canada Banff, Alberta, October, 2013.